2020

Altered Tyrosine Phosphorylation of Cardiac Proteins Prompts Contractile Dysfunction in Hypertrophic Cardiomyopathy

Mingguo Xu

Kevin C. Bermea

Marzieh Ayati

Xiaomei Yang

Zongming Fu

See next page for additional authors

Altered Tyrosine Phosphorylation of Cardiac Proteins Prompts Contractile Dysfunction in Hypertrophic Cardiomyopathy

Mingguo Xu[1,2,#], Kevin C. Bermea[1,#], Marzieh Ayati[3], Xiaomei Yang[4], Zongming Fu[5], Amir Heravi[1], Xinyu Zhang[6], Chan Hyun Na[7,8], Allen Everett[1], Kathleen Gabrielson[9], D. Brian Foster[10], Nazareno Paolocci[10,11], Anne M. Murphy[1] and Genaro A. Ramirez-Correa[12,1*]

[1]Department of Pediatrics/Division of Cardiology, [2]Department of Pediatric Cardiology, Shen Zhen Children's Hospital, Shen Zhen, China.[3]Deparment of Computer Science/College of Engineering and Computer Science, University of Texas Rio Grande Valley School of Medicine, Edinburgh, Texas.[4]Department of Anesthesiology, Qilu Hospital, Cheeloo College of Medicine, Shandong University, Ji'nan, 250012. China, [5]Department of Pediatrics/Division of Hematology, Johns Hopkins University School of Medicine, Baltimore, Maryland, USA. [6]Department of Cardiology, Qilu Hospital, Cheeloo College of Medicine, Shandong University, Ji'nan, 250012. China, [7]Department of Biological Chemistry/McKusick-Nathans Institute of Genetic Medicine, [8]Department of Neurology/Institute for Cell Engineering, [9]Department of Molecular and Comparative Pathobiology, [10]Department of Medicine/Division of Cardiology, Johns Hopkins University School of Medicine, Baltimore, Maryland, USA. [11]Department of Biomedical Sciences, University of Padova, Padova, Italy.[12]Department of Molecular Science/UT Health Rio Grande Valley, USA.

Running Title: *Enhanced Cardiac Protein's pTyr Influence Hypertrophy*

# These authors contributed equally.
*Corresponding Author:
Genaro A. Ramirez-Correa, MD/PhD
Department of Molecular Science
UT Health Rio Grande Valley
Research Building
5300 N L Street/ Office 1.408 McAllen, Texas 78502. USA
Phone: 956-665-2188
E-mail: genaro.ramirezcorrea@utrgv.edu

Abbreviations

HCM; Hypertrophic cardiomyopathy

DCM; Dilated cardiomyopathy

FHC; Familial Hypertrophic cardiomyopathy

cTnI; cardiac Troponin I

HF; Heart Failure

MHC; Myosin heavy chain

TnT; cardiac Troponin T

PKA; Protein kinase A

ErbB2; Erb-B2 Receptor Tyrosine Kinase 2 or Tyrosine Kinase-Type Cell Surface Receptor HER2

c-Src; SRC Proto-Oncogene, Non-Receptor Tyrosine Kinase

PTM; Post-translational modification

TMT; Tandem Mass tagging

AG-825;(*E*)-3-[3-[2-Benzothiazolythio)methyl]-4-hydroxy-5-methoxyphenyl]-2-cyano-2-propenamide or Tyrphostin AG 825, a selective ErbB2 inhibitor

EF; Ejection Fraction

FS; Fraction Shortening

MyBP-C; cardiac Myosin Binding Protein C

MLC3; Myosin Light Chain 3

Abstract

Altered Serine/Threonine phosphorylation of the cardiac proteome is an established hallmark of heart failure (HF). However, the contribution of tyrosine phosphorylation to the pathogenesis of these diseases remains unclear. The cardiac proteome was explored by global mapping to discover and quantify site-specific tyrosine phosphorylation in two cardiac hypertrophic models; cardiac overexpression of ErbB2 (TgErbB2) and cardiac expression of α–Myosin heavy chain R403Q (R403Q-αMyHCTg) compared to control hearts. Phosphoproteomic changes found in R403Q-αMyHC Tg mice indicated EGFR1, Focal Adhesion, VEGF, ErbB signaling, and Chemokine signaling pathways activity were likely to be activated. On the other hand, TgErbB2 mice findings displayed significant overrepresentation of Right Ventricular Cardiomyopathy, Hypertrophic Cardiomyopathy (HCM), and dilated cardiomyopathy (DCM) KEGG Pathways. In silico kinase-substrate enrichment analysis (KSEA) highlighted a marked downregulation of canonical MAPK Pathway Activity downstream of k-Ras in TgErbB2 mice and activation of EGFR, PP2 inhibition of c-Src, and Hepatocyte growth factor stimulation. *In vivo* ErbB2 inhibition by AG-825 decreased cardiac fibrosis, cardiomyocyte disarray, and rescued contractile function on TgErbB2 mice. These results suggest that altered tyrosine phosphorylation may play a regulatory role in cardiac hypertrophic models, suggesting that tyrosine kinase inhibitors could be used therapeutically in Hypertrophic Cardiomyopathy.

INTRODUCTION

Familial hypertrophic cardiomyopathy (HCM) increases the left ventricle (LV) wall thickness and cannot be explained by abnormal loading conditions. Mutations in genes encoding for sarcomeric proteins are common in HCM patients (40-60%)[1]. Studying post-translational modifications (PTMs) of sarcomeric (or Ca^{2+} handling proteins) can offer a unique opportunity to understand better how genetic disorders lead to cardiac dysfunction and discover potential targets for therapy [2-4]. For instance, PTMs of cardiac Troponin I (cTnI), a sarcomere protein that is centrally involved in myocardial contractility regulation, have been extensively studied, particularly for the functional role of PKA-dependent phosphorylation[5]. Notably, phosphorylation of cTnI-S22/23 - one of the most relevant regulatory sites of cTnI – is known to be down-regulated in human heart failure (HF)[6] and leads to contractile dysfunction [7].

Tyrosine phosphorylation is essential for cardiac structural development and myofibril organization during embryogenesis[8,9]. For example, several tyrosine phosphatases have been linked to heart disease and even proposed as a therapeutic target for some conditions. Moreover, mutations at the level of tyrosine-protein phosphatase non-receptor type 11 (PTPN11) can lead to HCM or dilated cardiomyopathy (DCM)[10,11]. In the heart, PTPN11 likely plays a role in systolic dysfunction produced by pressure-overload[12]. Another tyrosine phosphatase is associated with cardiac pathophysiology, specifically acid phosphatase 1 (ACP1):—the deletion of *ACP1* results in a protection against stress-induced cardiomyopathy [13]. Our group first showed that

cTnI-Y26 phosphorylation is readily detected in healthy human hearts and down-regulated in human HF and DCM [14]. However, how these alterations contribute to the onset and progression of cardiac disease remains poorly understood. A better grasp of additional site-specific changes of individual pTyr sites would help in this direction, substantially.

In the present study, a label-free and tandem mass tagging (TMT) quantitative global phosphotyrosine proteomics approach was applied to determine which sarcomeric sites have altered amounts of Tyr phosphorylation at specific sites in two unrelated models of HCM. The first model is secondary to the overexpression of the tyrosine kinase receptor ErbB2[15,16]; the second recapitulates features of the human disease, more specifically, an R403Q mutation of the myofilament protein myosin heavy chain, distinctive of familial hypertrophic cardiomyopathy[17]. The rationale for this choice was to determine whether triggering HCM through different mechanisms elicits similar, pTyr-related pathways/regulatory sites within the heart. In doing so, the manipulation of these Tyrosine phosphorylation sites can offer new opportunities for therapeutic targeting in different forms of human HCM

RESULTS

Choice of the Models

The approach combined examination of the global proteome and myofilament targeted tyrosine phosphorylation proteomics approach in two HCM mice models to identify the potential impact of altered Tyr phosphorylation on underlying disease mechanisms. One model has HCM caused by cardiac-specific overexpression of a tyrosine kinase receptor

(ErbB2); the second is a classic model of a point mutation in a significant sarcomeric protein (R403Q-αMyHC mice). TgErbB2 mice initially develop a striking, concentric cardiac hypertrophy, which evolves to diffuse fibrosis and myocyte disarray [16] with HCM. This line of mice also has abnormal calcium handling, and are prone to arrhythmias and develop Hypertrophic Obstructive Cardiomyopathy [2]. Similarly, R403Q-αMyHC mice reproduce human familial HCM by progressing from mild hypertrophy, mild fibrosis to frank myocyte disarray, HF, and arrhythmias [17].

Immunoblotting Reveals Increased Cardiac Tyrosine Phosphorylation in HCM models

First, immunoblot analysis of the myocardium of TgErbB2 and Ntg mice for tyrosine phosphorylation was applied. In the whole heart homogenates of ErbB2 overexpressing mice, there was a global increase of Tyrosine phosphorylation compared to non-transgenic (Ntg) littermates (Fig.1A). These findings were corroborated with an immuno-blot using pan-tyrosine phosphorylated antibodies detected by a fluorescent secondary and normalizing the tyrosine phosphorylation signal to Troponin I levels (Fig.1B). Although c-Src (proto-oncogene tyrosine-protein kinase Src) is downstream of ErbB2 signaling, we did not anticipate its increased expression in TgErbB2 mice (Fig1.C, D) when normalized to GAPDH signals. The c-Src activity was enhanced in TgErbB2 mice compared to Ntg, as revealed by enhanced Tyr416 phosphorylation (Fig.1E). Altogether these data suggest that tyrosine phosphorylation is a broadly distributed post-translational modification (PTM) in the myocardium. Therefore, alterations in cardiac tyrosine phosphorylation may play a regulatory role in the disease progression of non-ischemic

cardiomyopathies, such as familial cardiomyopathy (HCM) and dilated cardiomyopathy (DCM), as part of the pathophysiologic response to the underlying disease.

Tyrosine phosphorylation in myofilaments and cross-talk with serine/threonine kinases/phosphatases

A label-free phospho-tyrosine proteomics approach was undertaken to compare the cardiac tyrosine phosphorylation profile of Non-transgenic controls (Ntg), TgErbB2, and R403Q-αMyHC mice (Fig.2). It was hypothesized that unbiased global pTyr profiling would yield salient information about which specific tyrosine sites are phosphorylated in well-known essential cardiac-specific proteins and tyrosine kinases, thus providing clues about which tyrosine kinases could be mediating cardiac tyrosine phosphorylation. A total of 1,800 peptide spectra matched (PSM) were collected from the heart ventricle whole proteome, and 50% were identified with high confidence resulting in 431 unique tyrosine-phosphorylated peptides corresponding to 239 proteins. Tables with all identified phosphoproteins and phosphopeptides are provided in Supplementary Table 1-7. An evaluation of the MS data quality, intensity, and distribution post-median sweep normalization are shown in Supplementary Fig.S1. Confidence of Phosphorylated site localization was evaluated for annotation, and a score of more than 49% was required. This data set indicates that a comparable yield of peptide identification was achieved, reproducibility on the enrichment of pTyr peptides, and high-quality MS/MS data using similar approaches to others [18-20].

The label-free phospho-tyrosine proteomics approach core findings identified 239 different tyrosine-phosphorylated proteins, 169 tyrosine-phosphorylated proteins that overlap among the control mouse hearts (Ntg), and the myocardium from two cardiac hypertrophic models (TgErbB2 and R403Q-αMyHC). At the peptide level, 431 pTyr sites were detected with an overlap of 271 tyrosine phosphorylated residues (Fig.2E, F). Also, 18 novel pTyr sites were detected with an overlap of 13 pTyrosine sites for the three mouse groups (Fig.2G). These are novel sites not reported before, nor found in the extensively curated database PhosSitePlus (Cell Signaling Technology).

Next, the focus was on the cardiac-specific proteins from the myofilament apparatus. Nine major myofilament proteins were tyrosine phosphorylated. They harbor multiple tyrosine phosphorylation sites, many of which are novel (See Supplementary Fig.S2); the best example is Titin with 36 pTyr sites (See Supplementary Fig.S3). Also, seventeen tyrosine kinases had detectable tyrosine phosphorylation sites, and thus they could potentially be involved in regulating cardiac myofilament tyrosine phosphorylation.

In contrast, only two tyrosine phosphatases (Ptpn11 and Ptpra) demonstrated detectable tyrosine phosphorylation sites and, therefore, are likely to play a role in regulating cardiac tyrosine phosphorylation levels in the sarcomere. In addition to the number of tyrosine kinases found with pTyr sites, fifteen serine/threonine kinases had detectable tyrosine phosphorylation sites; however, only one serine/threonine phosphatase (Ppp1r12b) demonstrated tyrosine phosphorylation sites. These data show that cardiac myofilament tyrosine phosphorylation is broadly distributed and that there may be a cross-talk between tyrosine kinases/phosphatases with serine/threonine kinases/phosphatases.

ErbB2 Cardiac Overexpression and R403Q-αMyHC Point Mutation Remodeled the Cardiac Tyrosine Phosphorylation Proteome

Next, studies were undertaken to define the impact of ErbB2 cardiac overexpression and R403Q mutation of the cardiac myosin heavy chain on the specific tyrosine phosphorylation changes. Data were then analyzed to determine the signaling transduction pathways associated with two unrelated types of HCM. Spectral normalization and statistical methods were performed, as previously described [21,22]. Then, principal component analysis (PCA), k-means and hierarchical clustering were applied to determine if the pTyr profiles were similar within the groups. This approach determined that, indeed, the three groups segregate distinctively by the principal component 1 (PC1= 36.6%), whereas no group-wise distinction was evident in the second component (PC2=16.4%), see Fig.3A. Of note, one technical/biological replicate of R403Q-αMyHC was removed because it had more than 50% of absent pTyr peptides compared to the other two replicates. Hence, it was considered a technical failure. Heatmaps of hierarchically clustered up- or down-regulated pTyr peptides helped visualize the technical reproducibility and the specificity of how the genotype of cardiac hypertrophy largely influenced the phospho-tyrosine proteome remodeling (Fig.3B, $p<0.05$ by ANOVA). Tyrosine phosphorylated peptides are color-coded according to their extracted chromatogram MS1 signal intensities; yellow is upregulated, and blue is downregulated. This approach is a relative measure for peptide abundance. Additionally, k-means, which is an unsupervised machine learning algorithm, discovered the

underlying pattern, which is distinct to every group, see the clusters in Fig.3C ($p < 0.05$), as opposed to having a flat upregulated (green) or downregulated (red) line among the three groups. These results demonstrate that Ntg, TgErbB2, and R403Q-αMyHC mice each have a pTyr proteome with a distinct signature, evidenced by PCA, heatmaps clustering, and k-means analysis; all of which are unsupervised unbiased statistical methods.

Statistically significant changes (Log_2 fold change > 1, p-value<0.05) were detected in 28 phosphosites corresponding to 24 proteins in TgErbB2 mice (Fig.3D) and 77 phosphosites in 57 proteins in the R403Q-αMyHC Tg mice (Fig.3F) using ANOVA ($p < 0.05$). It is noteworthy that cardiac sarcomeric actin Y-200 was hyperphosphorylated (Log2 FC 1.11, $p < 0.05$) while cardiac Troponin I Y-113 was hypophosphorylated (Log2 FC -2.73, $p < 0.05$) on R403Q-αMyHC mice hearts. The statistically significant pTyr changes observed in both animal models were subjected to pathway analysis (Ingenuity Pathway Analysis, Qiagen®). However, IPA has well-known disadvantages since the results have to be subjectively interpreted by the user [23]. Statistical changes in proteins that match the phospho-tyrosine peptides do not account for the up-regulation or down-regulation of a peptide and how that impacts activation or inhibition of their activity within their respective pathway. The analysis yielded significant results about over-represented canonical pathways and their upstream master regulators (B-H corrected $p < 0.05$). Such as Tec Kinase Signaling, VEGF, integrin-linked kinase (ILK), Rho family GTPase, PAK, CXCR4, actin cytoskeleton, and cardiac hypertrophy signaling pathway for R403Q-αMyHC Tg mice, whereas that for TgErbB2 mice also actin cytoskeleton, ILK and

Synaptogenesis signaling pathway (Supplementary Fig.S4). However, since there are many pathways and potential master regulators, it is difficult to infer the precise biological significance. The complete list of upstream regulators is displayed in Supplementary tables 8 and 9 of Online Supplementary Data.

To circumvent IPA limitations, PhoshoEnrichment Software was used, which utilizes the Molecular Signatures Database (MsigDB) [24]. This database was created by the Broad Institute that comprehends a well-curated collection of annotated gene data sets. Also, a novel database of PTM site-specific phosphorylation signatures of kinases, perturbations, and signaling pathways (PTMsigDB) was employed. PTMSigDB was recently developed by the Broad Institute [25]. This tool accounts for phospho site-specific changes and their impact on activation or inhibition of a given pathway, together with the most common experimental Systems Biology Perturbations. The advantage of these bioinformatics tools is to assess the statistical significance of each pathway and Perturbation (gene-level and site-level) using a hypergeometric test. Here, the number of identified phosphosites and genes is used as the population for the hypergeometric model parameter instead of using all known genes as the population, as in IPA.

A pathway enrichment analysis was performed on significant genes/sites (Log_2 FC>1 and p-value < 0.05) using a gene-protein level with MSigDB. It was found that TgErbB2 mice's most significant pathways by KEGG are right ventricular cardiomyopathy (ARVC), see Fig.3D, E in pink color highlights, followed by hypertrophic cardiomyopathy (HCM) and dilated cardiomyopathy (DCM). Both Tg animal models showed a remarkable alteration

in Plakophilin-2 (PKP2) phosphorylation at the site Y119, although in TgErbB2 hearts, it was downregulated, and in R403Q-αMyHC Tg hearts, it was upregulated. Plakophilin-2 (PKP2) is a critical component of the myocardium's desmosomes, and mutations in the gene encoding for this protein are associated with arrhythmogenic cardiomyopathy [26-28], suggesting that disturbed phosphorylation could have a functional impact.

In comparison, the PTMsigDB revealed that pathway analysis at the phosphorylated site-specific level did not reach statistical significance for the EGFR1 pathway. In the case of TgErbB2 mice, only three site-specific phosphosites matched the EGFR1 pathway; they are highlighted in cyan color at the Volcano plot (Fig.3D) and PTMsigDB table (Fig.3E). Intriguingly, however, in R403Q-αMyHC mice, the same pathway was statistically significant; see the 16 site-specific changes that matched the EGFR1 pathway (p=0.001) represented in the volcano plot as cyan data points (Fig.3F) and PTMsigDB table (Fig. 3G). EGFR1 is a receptor tyrosine kinase, and the following most significant change is a signature secondary to Erythropoietin (PSP_EPO) stimulation ($p= 5.6^{-4}$); see three purple and one blue data points on the volcano plot (Fig.3F), the blue dot is to show an overlapping site, Stat5a Y694p, of EGFR1 pathway and PSP_EPO (Erythropoietin stimulation). These data show the utility of phosphorylation site-specific databases to narrow the search of a biologically relevant pathway on phospho-proteomics data sets, particularly in understudied phosphorylation events such as pTyr that have small data sets to date.

TMT Labeled Quantitative Proteomics of TgErbB2 Confirms Cardiac Sarcomere Tyrosine Phosphoproteome Dysregulation

A tandem mass tagging (TMT) quantitative labeling proteomics was used to gain more specific insight into the myofilament tyrosine phosphorylation changes. The hypothesis is that myofilament enrichment would enhance site-identification in myofilament proteins, specifically those with low abundance phospho-Tyrosine modifications, that may have been missed using the global approach. To that end, Ntg and TgErbB2 mice were evaluated using freshly isolated myofilaments, as described previously[29] with minor modifications, from three hearts per genotype and evaluated the tyrosine phosphoproteome (Fig.4A, B), as described previously for the Heart Failure phosphoproteome[20]. Briefly, in this 6-plex TMT experiment, the peptides identified with single spectra were removed, which lead to 24,727 peptide spectra matched (PSM). After median sweep normalization, there were 1,116 peptides that corresponded to 1,092 proteins. For spectral intensity distribution, before and after normalization, see Supplementary Fig.S5. For pTyr Proteome 4,391 PSM were collected and followed the same quality control curation of the full proteome to remove missing data and unique spectra, which led to 3,064 PSM. Raw data of pTyr proteome spectral intensity distribution and PCA are shown in Supplementary Fig. S6A. After median sweep normalization, 832 peptides corresponded to 184 different proteins. Specific tyrosine phosphorylation for 146 peptides was quantified because they had corresponding peptides from the full proteome's expression data. For further statistical data analysis, a workflow similar to that used for Label-Free proteomics was adopted. The only difference was that specific phosphorylation levels were calculated matching pTyr peptides intensity levels to their respective protein intensity levels on the flow-through fraction of peptides used for full

proteome determination and unsupervised statistical analysis obviated k-means because it is designed for experimental groups of three or more.

The first step of the analysis uses unsupervised principal component analysis (PCA) and hierarchical clustering. PCA analysis showed the correlation between members in the same group and the ellipse represent the confidence interval of 95% (See Fig.5A, B, C), full proteome, pTyr proteome, and normalized pTyr proteome segregate well along PC1, showing a correlation of expression of 53.9%, 47.2%, and 57%, respectively. Heatmaps of hierarchically clustered expression helped to easily visualize how TgErbB2 cardiac overexpression largely influenced the genotype clustering. Both patterns, proteins from the full proteome (Fig.5D), and the normalized intensity of pTyr Proteome (Fig.5E) suggested a mirrored remodeling (377 proteins for full proteome and 51 pTyr peptides had a $p < 0.05$ by LIMMA moderated 2-sample t-test comparison).

From the full proteome, 1116 peptides were detected, which corresponded to 1092 proteins. A comparison of the Log_2 fold-change (FC) of TgErbB2/Ntg showed 377 proteins with statistically significant differences (Log_2 FC >1 and p-value <0.05). Similar to label-free proteome data, the statistically significant protein expression changes were subjected to MSigDB for pathway analysis, and their results are shown in Supplementary Table 10.

To analyze specific pTyr Proteome specific phosphorylation, or normalized pTyr proteome, 146 phospho-sites that corresponded to 50 proteins were used, and the TgErbB2 mice showed significant changes in 21 pTyr sites (Fig.5G) that corresponded to 15 proteins. Of note, a significant increase of pTyr was detected on MLC1-Y82,139, Myh6-Y1310, α-Tm-Y261, Actin-Y168, MyBP-C-Y544, and Actinin2-Y200, among other

proteins. Once again, a pathway enrichment analysis was performed using MsigDB on the 15 proteins representing the 21 pTyr sites, and as in the case of the label-free approach, TgErbB2 mice most significant pathways by KEGG included DCM and HCM, see Fig.5G, H with magenta color highlights on volcano plot and table. Interestingly, when normalized to total ErbB2, the ErbB2-Y1006 phosphorylation levels are decreased. On the other hand, PTMsigDB pathways analysis did not match any pathways because many of those sites are new and not reported in the PTMsigDB database.

Kinase-Substrate Enrichment Analysis (KSEA) Implicated Downregulation of MAPK in TgErbB2 and Upregulation of EGFR in R403Q-αMyHCTg

Kinase-Substrate Enrichment Analysis (KSEA) was used to characterize genotype-induced signaling changes by estimating the kinase's relative activity in TgErbB2 and R403Q-αMyHC mice using the global pTyr label-free and TMT quantitative sarcomere pTyrosine proteomics data, using their respective Ntg groups as a reference. KSEA [30] is a method that infers the kinases' differential activity based on the differential phosphorylation of its substrates and computes scores that reflect the directional change in each kinase's signaling. This method assumes that the differential activity of kinases is correlated with phosphorylation changes in its substrates. A positive score corresponds to a kinase with phosphorylated substrates in Tg mice relative to Ntg control. Likewise, a negative score is a hypophosphorylation in Tg relative to their Ntg control. The kinase-substrate interaction data was downloaded from the PhosphoSitePlus (PSP) [31] website. Next, the KSEA method was applied to all the pTyr sites identified in these experiments.

This resulted in the identification of 27 phosphosites that have associated kinases reported on PhosphoSitePlus. However, a total of 58 unique kinases were scored in the combined data sets. A KSEA heatmap inferred clusters of kinases downregulated (blue color scale) or upregulated (red color scale) is shown in Fig.6A, both TgErbB2 and R403Q-αMyHC Tg mice displayed an inferred downregulation of MAP3K6, MAP3K5, and MAPK14, whereas TgErbB2 showed an additional downregulation of MAP2K6, MAP2K4, TYK2, and RET see highlighted blue rectangle on Fig.6A. Most of them belong to the canonical MAPK pathway downstream of k-Ras.

On the other hand, R403Q-αMyHC Tg displayed an inferred upregulation of Src, LYN, LCK, JAK2, INSR, MAPK1, and HCK, which annotate to Focal Adhesion, VEGF, and PDGFR-beta signaling pathways. For example, see the highlighted red rectangle in Fig.6A. Altogether these KSEA results suggest that TgErbB2 and R403Q-αMyHC mice had a differential kinase activity signature, where TgErbB2 shows downregulation of MAPK Pathway and R403Q-αMyHC has an up-regulation of Focal Adhesion, VEGF, and PDGFR-beta signaling pathways, which are sharply different cellular responses.

Since the pathway enrichment analysis of pTyr TMT data did not yield further insights distinct from label-free pTyr data, a protein-protein interaction (PPI) network approach was employed. Pathway analysis can miss protein groups mainly because pathways algorithms are predefined and rigid. PPI might better capture signaling responses in these models that are not classically detected by pathway analysis. To do so, MoBaS Analysis[22,32] was employed, i.e., to identify densely-connected subnetworks that are related and might exhibit differential phosphorylation in Tg models. Several modules were identified and focus on the top two most statistically significant PPI

modules from the label-free data set; for purposes of interpretation, they were designated as Module 1 and Module 2. The substrates of Modules 1 and 2 are illustrated in Fig.6B and Fig.6D, respectively. Interestingly, PTMsigDB site-level molecular signature analysis showed that Module 1 contained site-specific modifications statistically significant for Hepatocyte Growth Factor (HGF) perturbation and Thyroid Stimulating Hormone (TSH) Pathway (highlighted in light blue). In addition, using MSigDB Gene-Protein Level analysis, several pathways, such as the VEGF1/2 pathway, highlighted in yellow in the PPI module (Fig.6B, F) showed statistical significance. Also, PTMSigDB analysis for Module 2 revealed a significant match with PP2 Perturbation (c-Src family kinases inhibitor PP2), which is highlighted in blue in Fig.6D and Fig.6F, and with EGF Perturbation (PTMsigDB defines it as a systems biology response to EGF Stimulation). Next, KSEA was applied to the identified modules by restricting the analysis to the target pTyrosine sites of kinases that are present in the protein-protein interaction Modules 1 and 2. In Fig.6C, the comparison of kinases altered activity between datasets of Module 1 substrates is displayed. In this analysis, R403Q-αMyHC mice have a marked significant upregulation of PTK6, PTK2, FYN, ABL1, KDR, CSNNK2A1, and AURKB (denoted by white asterisk $p<0.05$), which form part of Integrin Signaling Pathway (ABL1, FYN, PTK2) and VEGF Pathway (KDR and PTK2). Likewise, in Module 2 substrates, the kinase activity is significantly increased in R403Q-αMyHC mice, see Fig.6E, significant kinases denoted by white asterisk ($p <0.05$). Of note, some of these altered kinases belong to Finetti Breast Cancer Kinoma, PDGFR-beta Signaling Pathway, PTP1B Pathway, and ErbB2/3 Pathway from MSigDB (See Fig.6E). Altogether these results confirm that MoBAS identified functionally relevant modules of protein-protein interactions (PPI)

among identified pTyr peptides and pointed insights into system biology processes from PTMsigDB that were not detected on global analysis.

Tyrphostin AG-825 administration decreased cardiac fibrosis, cardiomyocyte disarray and preserved contractile function in the TgErbB2 mouse model

Although TgErbB2 mouse hearts develop a concentric type of HCM, this rapidly progresses to pathologic HCM and shows histopathological features of HCM, including fibrosis, cardiomyocyte disarray, perturbed Ca^{2+} handling, arrhythmias, and sudden death [16]. It was hypothesized that by counteracting the activity of cardiac ErbB2 overexpression pharmacologically, a tyrosine kinase receptor, by using AG-825 (an ErbB2 inhibitor), would halt the progression of the histopathological phenotype. To that end, TgErbB2 mice with established HCM and Ntg controls were treated with AG-825 or DMSO vehicle for two weeks, subcutaneously twice daily at a dose of 1mg/Kg [16]. Next, myocardial fibrosis was evaluated by Masson's trichrome staining. Untreated TgErbB2 mice developed variable amounts of fibrosis of the left ventricle (Fig.7A, B, lower left panels); however, TgErbB2 treated mice displayed less fibrosis (Fig.7B, lower right panels).

In contrast, cardiac histology was not affected by AG-825 treatment in Ntg mice. To characterize the effects of AG-825 on cardiomyocyte disarray CytoSpectre [33], a web graphic user interphase (GUI) was employed, this interphase determines the local orientation of structures, including cardiac myocytes, across histological sections, similar to the analysis described previously by Seidman Lab [34]. Randomly chosen regions of interest (ROI) are depicted in Fig.7A and increase the magnification of microphotographs

from 5X to 40X (See Fig.7B). The myofiber orientations angle variance was defined is referred to as Circular Variance from Ntg treated with the vehicle, see Ntg-Vehicle in Fig.7C top left panel, and then compared the cardiac myocytes' orientation angles variance from Ntg AG-825 treated (Fig.7C top right panel), which was not significantly different (Fig.7D), as described previously [34]. In contrast, TgErbB2 mice cardiomyocytes treated with the vehicle displayed an orientation angle variance that was significantly different from Ntg-Vehicle control; see the heterogeneous and broader shape of the orientation plot in Fig. 7C, lower-left panel. Surprisingly, cardiomyocytes from TgErbB2 mice AG-825 treated displayed significantly less disarray, as demonstrated by the significant return of circular variance and shape of the plot to Ntg- Vehicle or AG-825 treated controls, see Fig.7E. This analysis confirms that cardiomyocytes from TgErbB2 mice AG-825 treated displayed significantly less myocyte disarray, as indicated by reduced circular variance.

Lastly, to study the direct *in vivo* effects of ErbB2 inhibition by AG-825 on contractility, echocardiograms, and tissue-doppler imaging (to evaluate diastolic function) was performed on conscious mice (non-anesthetized) at baseline and after two weeks of treatment. A Vevo 2100 High-Resolution Imaging System with a 40MHz transducer (VisualSonics®, Toronto) was used, and the data were subsequently analyzed with an Advanced Cardiovascular Package Software. The parameters analyzed were chamber dimensions, fractional shortening, ejection fraction, and tissue Doppler velocity dynamics. LV functional data obtained by parasternal short-axis echocardiographic imaging determined a significant decrease in the mean fractional shortening over time in TgErbB2 mice treated with vehicle solution compared with the Ntg (Ntg 57.19% ± 2.25 vs. TgErbB2

43.72% ±5.05, p-value < 0.05). In contrast, TgErbB2 mice treated with AG-825 did not display a significant decline in contractile function over time when compared to Ntg AG-825 treated (TgErbB2 50.3% ±5.94 vs. Ntg 58.95% ± 2.35, p-value > 0.05). Also, the ejection fraction (data not shown) of the TgErbB2 mice treated with the vehicle was significantly lower than Ntg (TgErbB2 68.07%±5.64 vs. Ntg 81.60% ± .95); this decline in contractility was abolished by AG-825 treatment of ErbB2 Tg mice (TgErbB2 74.86% ±5.76 vs. Ntg 83.09% ± 1.93). TDI detected no additional beneficial effects on diastolic function; see complete Echocardiography data on Supplementary Table 11. Altogether, these data suggest that ErbB2 pharmacological inhibition halted or reversed pathological remodeling by reducing the fibrotic response and restoring cardiomyocyte alignment, further reflected by an *in vivo* preservation of LV contractile function without effect on LVH from TgErbB2 mice.

DISCUSSION

This study demonstrates that cardiac-specific overexpression of ErbB2 and allelic expression of R403Q-αMyHC alters the tyrosine phosphoproteome of the cardiac sarcomere and signaling pathways related to hypertrophic cardiomyopathy (HCM). In the TgErbB2 mouse model, a total of 51 tyrosine-phosphorylated sites were significantly altered, with 28 up-regulated peptides and 23 down-regulated peptides (Log_2 FC > 1.0, p < 0.05). Among those 51 sites, 7 (Myh6-Y1261, Myh6-Y1349, Ttn-Y2118, Ttn-Y21190, Ttn-Y31324, Sgcb-Y46, and ATP2a2-Y497) belong to proteins involved in both the hypertrophic cardiomyopathy (HCM) and dilated cardiomyopathy (DCM) KEGG

pathways. Significant alterations were observed in the elements of the right ventricular cardiomyopathy (ARVC) KEGG pathway. Interestingly, a greater number of tyrosine-phosphorylated sites were significantly altered in R403Q-αMyHC mice compared to TgErbB2 mice (78 vs. 51, respectively; Log_2 FC >1.0, $p<0.05$), including 48 upregulated phosphosites and 30 downregulated phosphosites. Conversely, the total number of tyrosine-phosphorylated sites identified in both mouse models was similar (TgErbB2 n=348 vs. R403Q-αMyHC *n*=352, Fig.2F). This evidence suggests that the differences observed can be attributed to genotype or phenotype differences between these two mouse models. Interestingly, we unearthed the same HCM/DCM tyrosine-phosphorylated peptides in TgErbB2 mice and R403Q-αMyHC mice. However, only on R403Q-αMyHC mice, the changes reached statistical significance for HCM/DCM KEGG pathways' involvement. Some of the pathways highlighted by the KSEA in R403Q-αMyHC Tg mice include the Focal Adhesion, VEGF, ErbB signaling, Chemokine Signaling, and Angiopoietin receptor pathways.

Initially, it was reasoned that overexpression of a receptor tyrosine kinase in TgErbB2 mice hearts would result in a more significant alteration of tyrosine phosphoproteome. However, the data suggest that a single sarcomere point mutation, as in the case of R403Q-αMyHC mice, is enough to alter the cardiac tyrosine phosphoproteome significantly. Another surprising finding was that the ErbB signaling pathway elements were not significantly altered in TgErbB2 mice, but rather in R403Q-αMyHC mice. Indeed, MSigDB analysis in the TgErbB2 mice yielded only two targets (CRK and SHC1) associated with the ERBB Signaling KEGG pathway. The TgErbB2 mouse model is important because it shows pronounced cardiac hypertrophy at an early

age, sarcomere dysfunction, and abnormal calcium handling [16], thus connecting the tyrosine kinase pathway and tyrosine phosphorylation to cardiac hypertrophy. While ErbB2 was previously reported to be overexpressed ~40-fold in TgErbB2 hearts [12], the tandem mass tagging quantitative proteomics data, which allowed normalization of the peptide phosphorylation signal to total protein levels of ErbB2, revealed that the phosphorylation level of ErbB2-Y1006 peptide is reduced in this model (Fig.5G). The low stoichiometry of phosphorylated:non-phosphorylated ErbB2 may account for the apparent lack of alteration of the ErbB signaling pathway.

In contrast, R403Q-αMyHC exhibited alterations in eight members (CRK, GSK3B, MAPK1, MAPK3, NCK1, PTK2, STAT5A, and STAT5B) of the same pathway (Fig.3G). The mechanisms by which a pathogenic mutation in the myosin heavy chain may affect tyrosine phosphorylation regulation is unknown and warrants further investigation.

On the other hand, pharmacological inhibition of ErbB2 (HER2/neu) with the inhibitor lapatinib in breast cancer patients treated with doxorubicin increases the risk of developing heart failure compared to patients treated with doxorubicin alone [35]. This finding suggests that maintaining homeostasis of tyrosine phosphorylation may be important for regulating cardiomyocyte function and homeostasis.

EGFR1 pathway is central to HCM

The EGFR1 (ErbB1) Pathway seems to play a central role in cardiac hypertrophy in both Tg models. However, at the site-specific level, the molecular signature (PTMsigDB) of R403Q-αMyHC had 16 specific peptides altered consistent with the activation of the EGFR1 pathway. The TgErbB2 mice tyrosine-phosphorylated peptides did not reach

statistical significance, with only three specific peptides for PTMsigDB (Fig.3E, G). EGFR pharmacological inhibition, using AG-1478, protects against Angiotensin II-induced cardiac hypertrophy in vitro and in vivo [36]. The concentric hypertrophy associated with ErbB2 cardiac-specific overexpression can be reversed by early administration of Lapatinib, which inhibits EGFR receptor Tyrosine kinase [12] in addition to ErbB2. In this study, the ErbB2 receptor's pharmacological blockage by the small molecule inhibitor AG-825 in TgErbB2 adult mice preserved cardiac function without affecting cardiac hypertrophy. In addition, the specific blockage of ErbB2 by AG-825 reduced myocyte disarray and cardiac fibrosis. These findings indicate some overlap in cardiac hypertrophy signaling mediators downstream of EGFR1 and ErbB2, and the sarcomeric mutation R403Q-αMyHC appears to amplify the EGFR Signaling Pathway preferentially.

Tyrosine phosphorylation is present in multiple proteins associated with the regulation of cardiac function and disease

A wide variety of other functionally relevant targets were identified in this study as tyrosine phosphorylated, from sarcomere proteins to Z-disk and desmosome components, focal adhesion, and adherence junction proteins, membrane receptors, kinases, and phosphatases. For instance, tyrosine phosphorylation in several Z-disk associated proteins was noted (For a full list, see Supplementary tables 2-7). Z-disk proteins are crucial for muscle contraction and mechanical stress, growth, and metabolic signaling [37]. Also, the alteration in the phosphorylation levels of the desmosome key component Plakophilin-2 protein (Pkp2) peptide Pkp2-Y119 was noted in both mouse models, up-regulation in R403Q-αMyHC Tg and down-regulation in TgErbB2. The functional effect of

up- or down-regulation of Pkp2-Y119 phosphorylation is not known. However, Pkp2 homozygous deletion disrupts heart architecture and is lethal in the embryo [38]. In the heart, Pkp2 is required for the assembly of the desmosome and the PKC activity [39]. Autosomal dominant mutations in this gene are responsible for 25% to 50% of arrhythmogenic cardiomyopathy (ARVC). Interestingly, TgErbB2 mice have increased susceptibility to arrhythmias and myofibrillar disarray [16], similar to patients with myosin mutations and HCM. Pkp-Y119 phosphorylation changes could impact the phenotype.

Bioinformatic Identification of Potentially Activated Kinases that are Drug Targets

The *in silico* kinase-substrate enrichment analysis (KSEA) implicated a marked downregulation of members of canonical MAPK Pathway downstream of k-Ras in TgErbB2 mice, whereas, in R403Q-αMyHC mice, an up-regulation of Focal Adhesion, VEGF, and PDGFR-beta signaling pathways (SRC, LYN, LCK, JAK2, INSR, MAPK1, and HCK) was observed. More importantly, modularity-base scoring (MoBas) analysis demonstrated protein-protein interaction networks that by PTMsigDB identified Hepatocyte Growth Factor perturbation (or stimulation), PP2 Perturbation (effect of a c-Src inhibitor), and EGF perturbation (or stimulation). These data demonstrate that many targets overlap in both transgenic models of cardiac hypertrophy and although there are marked differences in the upstream regulators of ErbB2 and myosin heavy chain, many of the downstream effector molecules are common and can be targeted by small-molecule inhibitors (designed initially to treat several types of cancer) to block cardiac hypertrophy.

The MAPK pathway is involved in the adaptive and maladaptive response that could lead to heart hypertrophy (for review [40]). The RAS-RAF-MEK-ERK signaling pathway is an attractive target for therapeutic intervention in oncology, and several selective RAF and MEK small molecule inhibitors have been tested in clinical trials [41]. The present study found increased phosphorylation at MAPK1-Y185, which activates the kinase, in R403Q-αMyHC, and MAPK1 activity directly relates to heart hypertrophy [42]. c-Src figures as one of the potential regulators for the phosphotyrosine proteome changes observed in R403Q-αMyHC because it phosphorylates the EGFR receptor upstream and phosphorylates Stat, among other targets, downstream. c-Src affects the response to mechanical cardiomyocyte stretching by triggering a cascade of intracellular signaling in cardiomyocytes towards a hypertrophic response [43,44]. Also, c-Src phosphorylates PXN-Y118 [45], and this site had a 25-fold increase in phosphorylation in R403Q-αMyHC mice. Interestingly, c-Src mediates the activation of MAPK1 and MAPK3 in response to pressure overload [43]. Notably, a previous study has shown that pressure overload-induced cardiac hypertrophy is exacerbated in R403-αMyHC Tg mice [46], suggesting that the mechanism by which R403-αMyHC mutation produces heart hypertrophy might be by sensitizing cells to pressure-overload induced signaling via c-Src.

R403Q-αMyHC mice displayed enhanced JAK2, STAT5A, and STAT5B phosphorylation in the activation sites (Y570, Y694, and Y699, respectively), which indicates not only activation of MAPK signaling but also activation of JAK-STAT signaling. Jak-Stat Signaling: IL-6 pathway is activated in response to the IL-6 family of cytokines (IL-6, cardiotrophin 1, and leukemia inhibitor factor), cross-talks with the EGFR pathway, and is

involved in cardiac hypertrophy. This pathway has cardioprotective effects, but chronic activation may lead to heart hypertrophy (for review [40]). Vakrou et al. performed a pathway analysis on miRNA profiles of R403Q-αMyHC. They found similarities with the findings described in this work (For IPA data, see Supplementary Fig.S4, Supplementary Table 9), such as overactivation of integrin-linked kinase (ILK), IL-8, Rho family GTPase, PAK, CXCR4, actin cytoskeleton, and cardiac hypertrophy signaling pathways [47]. It is known that the integrin-linked kinase signaling pathway is over-activated in heart hypertrophy [48]. Altogether, these results suggest an essential involvement of Tyrosine phosphorylation regulation in myofilaments and other cardiac proteins. The insight gained from these studies could inform new therapeutic approaches in sarcomere mutation related HCM as well as potentially other conditions associated with HCM.

Limitations & Studies in Perspective

The studies were limited to two transgenic mouse models that develop cardiac hypertrophy; other models of sarcomere mutations or pressure overload such as aortic banding could be explored and compared. Some relevant tyrosine-phosphorylated sites might be missed due to their low stoichiometry and technical challenges. This problem is particularly true for membrane-bound proteins, which are difficult to evaluate in phosphoproteomic studies.

Conclusions

This study reveals that altered patterns of Tyrosine phosphorylation are striking in two separate models of hypertrophic cardiomyopathy. Moreover, despite some shared sites,

etiologically different forms of HCM may harbor specific tyrosine phosphorylation signatures. This evidence, combined with inhibition of a specific receptor tyrosine kinase using tyrphostin AG-825, can reverse cardiomyocyte disarray, thus preserving function in a TgErB2 mouse HCM model, could rationalize approaches to manipulate the Tyr phosphoproteome as a therapeutic approach for HCM in general. Furthermore, these studies indicate that tyrosine kinase inhibitors, now used broadly in cancer therapies, may change cardiac function by directly modifying the heart's tyrosine kinase profile.

METHODS

Western blot

Whole heart lysates from Heat Stabilized Tissue were resuspended in 1% SDS buffer, 10-15 μg were separated by SDS-PAGE, and transferred to nitrocellulose membranes. Membranes were blocked with 5% BSA in TBS-T buffer (20 mmol/L Tris pH 7.4, 150 mmol/L NaCl and 0.05% Tween 20) for 1h at room temperature, then were incubated with primary antibody (Anti-pTyr mouse monoclonal 1:2000, Anti-SRC, Anti-pSRC Y416, Anti-GAPDH 1:1000 dilution, Cell Signaling, Anti-cTnI 1:5000) at 4°C overnight. After washing them five times, the secondary antibody (goat anti-mouse-HRP, goat Anti-mouse IRDye® 800CW or goat Anti-rabbit IRDye® 680 LT 1:10,000) was added and incubated for 45 min. Then, the membranes were developed with super signal West Pico Chemiluminescent Substrate (Thermo), and the immunoreactive bands were detected by chemiluminescence system (Bio-Rad) or by Odyssey (Li-Cor). The images were obtained with Odyssey Software, and the quantifications were performed with Image J software.

Label-Free Proteomics

Sample Preparation Label-Free: All protocols were performed following the "Guide for the Use and Care of Laboratory Animals" published by the National Institutes of Health and the Institutional Animal Care and Use Committee's approval. To establish breeding colonies, the TgErbB2 and R403Q-αMyHC mice were obtained from Dr. K. Gabrielson and Dr. L. A. Leinwand, respectively [16,17]. Mice were anesthetized with sodium pentobarbital IP (75 mg/kg) or isoflurane (5%) overdose; the hearts were quickly dissected, followed by thermal stabilization (Denator T1 Heat Stabilizor, Sweden) and stored at -80°C until analyzed. TgErbB2 and R403Q-αMyHC mice hearts (n=5 per group) were processed in parallel. To obtain whole heart lysates, cardiac ventricles (~200 mg) were homogenized on ice-cold buffer: 20 mM HEPES, pH 7.6, 1mM, 1.5 mM sodium pyrophosphate, PhosStop, and 9M urea at 10 µl/mg (wet weight of tissue). The homogenate was cooled on ice, followed by brief micro-tip sonication on ice, centrifugation at 10,000 × g for 15 min at 4 °C. The supernatant was retrieved, and protein concentration was determined by the method of Lowry (Bio-Rad).

Trypsin Digestion: Protein from heart lysates was reduced in 5 mM of dithiothreitol (DTT), 60 °C for 20 minutes, and alkylated in 10 mM iodoacetamide (IDA) at room temperature for 15 minutes in the dark. Each sample (30mg per mouse, n=5 mice per genotype) was digested with Proteomics grade Trypsin (Promega) at a ratio of 1:200 in 2M urea, 20mM HEPES buffer, pH 8.0 at room temperature overnight. The digestion was terminated with trifluoroacetic acid (1% TFA). Samples were centrifuged (5 min at 1800g), and supernatants were desalted by solid-phase extraction (SepPak C18 10cc cartridge, Waters). Elutes were lyophilized for three days at -20°C.

Enrichment of Tyrosine Phosphopeptides: A total of 150 mg of trypsinized peptides per genotype were pooled and enriched for pTyrosine, as previously described [49]. Lyophilized peptides were mixed in 1.4 ml immunoprecipitation buffer (IAP buffer 50mM MOPS, pH 7.2, 10mM sodium phosphate, 50mM NaCl, pH 7.0. A stock solution of protein agarose G beads (Santa Cruz Biotechnology) 80µL of slurry were conjugated with 300µg of Phospho-Tyrosine Mouse monoclonal antibody (p-Tyr-100, Cell Signaling Technology). The beads-Anti-p-Tyr antibody conjugate was transferred to the peptide's tube and incubated with gentle rotation for 2h at 4°C. The beads were washed and eluted with 55 µl and 45 µl of 0.15% trifluoroacetic acid (TFA), respectively. The two elution yields were pooled. The resulting peptide mixtures were purified by solid-phase extraction (stage tips C18, Thermo Scientific). The samples were dried by vacuum centrifugation. This approach was repeated three times with samples from all three groups run in parallel, 15 hearts per genotype in three technical replicates.

LC-MS/MS Analysis: Phosphopeptides were dissolved in 10µl of 0.1% TFA, 2%ACN (v/v) followed by RF-HPLC-ESI-MS/MS analysis. Phosphopeptides were separated on a C18 reversed-phase column with a linear gradient of acetonitrile (4−40%) for 120 min and then analyzed on an LTQ-Orbitrap Elite MS (ThermoFisher Scientific) with neutro loss triggered HCD.

Peptide Identification, Quantification, and Statistics: Raw MS data were searched with Mascot 2.3, and label-free quantification with MS1 extracted ion chromatograms were performed using MaxQuant software. For statistical analysis, we followed the workflow of Foster et al. [21], with few modifications. First, Partek software was used to calculate the p-values, q-values, fold change, and ratio for each peptide intensity.

Phosphosites with less than 50% of missing density values were subjected to statistical analysis and the reminding missing values were filled with the K-nearest neighbors. Then, a normalization of the Log_2 densities by median subtraction and determined the fold-change, ratio, and statistical significance (q and p values), from each of the selected phosphosites of the data set. The volcano plots were made with GraphPad Prism 7®. Unsupervised principal component analysis (PCA) was used in both data sets separately with Partek® software. Data set segregated along with each component concerning the pTyr abundance (normalized, mean=0, variance=1). For K-mean clustering and unsupervised hierarchical clustering, Spotfire® software was used.

Tandem Mass Tagging Phospho Tyrosine Proteomics

Sample Preparation and TMT pTyr Enrichment: Myofilament proteins (~7 mg) from mouse heart were resuspended in 8 M urea and 50 mM triethylammonium bicarbonate (TEAB) (Sigma) followed by reduction with 10 mM dithiothreitol (Sigma) at room temperature for 1 h and alkylation with 30 mM iodoacetamide (Sigma) for 20 minutes in the dark. The protein samples were then digested overnight at 37 °C using sequencing grade trypsin (1:50) (Promega). Tryptic peptides were desalted and labeled with 6-plex isobaric tandem mass tags (TMT) (Thermo Scientific) according to manufacturer's instructions. The labeling reaction was carried out for 1 hour at room temperature, followed by quenching with 100 mM Tris.HCl (pH 8.0). The digested and labeled peptides were pooled and desalted with C_{18} SEP-PAK (Waters), followed by pTyrsoine enrichment using PTMScan® Phospho-Tyrosine Rabbit mAb (P-Tyr-1000) kit (Cell Signaling Technology). Briefly, the desalted peptides were reconstituted in 1.4 ml

of immuno-affinity purification (IP) buffer containing 50 mM MOPS pH 7.2, 10 mM sodium phosphate, 50 mM NaCl. Anti-phosphotyrosine antibody (P-Tyr-1000, Cell Signaling Technology) was mixed with peptide solution and incubated on a rotator at 4°C for 2 h. After incubation, the beads were washed with IP buffer and water for two and three times, respectively. The phosphotyrosine peptides were eluted using 0.1% TFA. The eluted peptide samples were desalted using C18 STAGE tips, vacuum dried, and kept at −80°C before LC-MS analysis. From flow-through, a quantification of the full proteome was made to serve as a reference for pTyr proteome findings.

LC-MS/MS Analysis: The phosphotyrosine peptides were analyzed on Orbitrap Fusion Lumos Tribrid (Thermo Scientific, San Jose, CA, USA) coupled with Easy-nanoLC 1200 nanoflow liquid chromatography system (Thermo Scientific). The peptides from each fraction were reconstituted in 10% formic acid and loaded on Acclaim PepMap100 Nano Trap Column (100 µm × 2 cm) (Thermo Scientific) packed with 5 µm C_{18} particles at a flow rate of 5 µl per minute. Peptides were resolved at 250 nl/min flow rate using a linear gradient of 10 to 35% solvent B (0.1% formic acid in 95% acetonitrile) over 95 minutes on the EASY-Spray column (50cm x 75µm ID, PepMap RSLC $C_{18,}$ and 2µm C_{18} particles) (Thermo Scientific) and it was fitted on EASY-Spray ion source that was operated at 2.0 kV voltage. Mass spectrometry analysis was carried out in a data-dependent manner with full scans in the range of m/z 350 to 1500. Both MS and MS/MS were acquired and measured using Orbitrap mass analyzer. Full MS scans were measured at a resolution of 120,000 at *m/z* 200. Precursor ions were fragmented using a higher-energy collisional dissociation method and detected at a mass resolution of 30,000 at *m/z* 200.

Peptide search, Identification, and Statistics*:* MaxQuant 1.5, or the most current version, was used for quantitation and identification against a mouse RefSeq database (version 78) supplemented with frequently observed contaminants. The search parameters used are as follows: a) trypsin as a proteolytic enzyme (with up to two missed cleavages) b) peptide mass error tolerance of 10 ppm; c) fragment mass error tolerance of 0.02 Da; d) Carbamidomethylation of cysteine (+57.02Da) and TMT tags (+229.16 Da) on lysine residue and peptide N-termini as fixed modification and oxidation of methionine (+15.99 Da) and phosphorylation of serine/threonine/tyrosine (+ 79.96 Da) as variable modifications. Two missed cleavages were allowed and 'match between runs' was enabled. Peptides and proteins were filtered at a 1% false discovery rate. Proteins with a q-value lower than 0.05 will be considered as differentially expressed with statistical significance. In a complementary way, R software was used. A two-sided t-test and the moderated p-values and q-values calculation was performed using an algorithm developed by Herbrich et al [50].

Systems Biology Analysis

Statistical analysis of the label-free data set was performed using Perseus software [51]. Peptides with less than 50% of detection were filtered and the missing values of the intensities of the reminding peptides were filled with k-nearest neighbors. Then, the log2 intensities were normalized by mean subtraction subsequently ANOVA and false discovery rate calculations. The K-mean clustering with Spotfire, 4 clusters were made using correlation as similarity measurement and data centroid based search. A heatmap was used to visualize the unsupervised hierarchical clustering of proteins with p-value <0.05 by ANOVA test.

The web-based software Ingenuity Pathway Analysis (IPA) was used for both data sets for pathway analysis. The results obtained were uploaded to IPA software. The Uniprot Accession ID was selected as an identifier for each site, and the cut of values for each intensity was a p-value < 0.05 and an absolute fold change of 2. Interaction networks were generated, including endogenous chemicals with 70 molecules per network and 25 networks per analysis. All node types and data sources were selected, considering all experimentally observed and predicted (high and moderate confidence) in all species.

Pathway Enrichment Analysis: The hypergeometric p-value was used to identify the processes that are significantly enriched in the proteins and phosphosites that are differentially phosphorylated between case and control samples. For this purpose, MsigDB [24] was used to analyze the protein level pathways and PTMsigDB [25] to analyze the processes at the site level. The population/background for which the enrichment is calculated against is restricted to all the proteins in which their sites are quantified in the phosphoproteomics experiment, rather than all universally known proteins/phosphosites.

Kinase-Substrate Enrichment Analysis (KSEA): Kinase Substrate Enrichment Analysis seeks to identify kinases whose targets exhibit significantly altered phosphorylation levels in a given condition. KSEA scores each kinase k with a set of substrates S as follows:

$$score(k) = \frac{(\bar{P}_S - \bar{P}) * \sqrt{|S|}}{\sigma}$$

Where, $\bar{P}_S$ Denotes the average $\log_2$ of fold change of all the substrates of kinase k, and $\bar{P}$ and σ represent the average and standard deviation of $\log_2$ of fold change of all the identified phosphosites in the dataset, respectively. KSEA was performed on the identified modules by restricting S to the substrates in the module instead of all substrates in the dataset. The data provided by PhosphoSitePLUS [31] was used as the reference for kinase-substrate associations. This tool is also available to download from compbio.case.edu/phosphoxplorer.

Module Identification: First, networks were created in which nodes represent proteins and edges represent the protein-protein interaction (PPI) obtained from BioGRID [22,52]. The proteins were assigned a score in the networks by computing the average fold change of phosphosites residing on each protein obtained from experiments individually (i.e., Ntg, TgErbB2, and R403Q-αMyHC Tg). Then MoBaS [22] was applied to identify sub-networks of proteins that are highly connected and differentially phosphorylated. For visualization of subnetworks, if a protein in one dataset is not identified in another dataset, the node is represented in grey color.

Echocardiogram: Cardiac morphology and function were assessed by transthoracic echocardiography using a high-resolution high-frequency system (Vevo 2100, VisualSonics, Canada) equipped with 40 MHz ultrasound probe in conscious mice as described previously [22,53]. Mechanical and chemical chest hair removal was performed by shaving and using a commercially available depilatory agent. Core temperature, monitored via a rectal probe, was maintained at 36.5-37ºC using a heating lamp. Parasternal long and short-axis views of the heart were captured in both B-and M-modes

at optimized frame rates. LV end-diastolic (LVIDd, mm) and end-systolic (LVIDs, mm) internal diameters, the end-diastolic wall thickness of both interventricular septum (IVS, mm) and LV posterior wall (LVPW, mm), LV ejection fractions (EF, %) and fractional shortening (FS, %) were measured using M-Mode in long-axis view. Relative wall thickness (RWT), a measure of hypertrophy, was calculated as IVSd+LVPWd/LVID. Pulsed-Doppler recordings at the mitral inflow, left ventricular outflow, and basal septum was recorded. Digital images were stored and analyzed off-line using commercially available Vevo LAB software (VisualSonics, Canada). An experienced echocardiography technician blinded to experimental groups performed all the measurements.

References

1 Hershberger, R. E. *et al.* Genetic evaluation of cardiomyopathy: a clinical practiceresource of the American College of Medical Genetics and Genomics (ACMG). *Genetics in Medicine* **20**, 899-909, doi:10.1038/s41436-018-0039-z (2018).

2 Sørensen, L. L. *et al.* Echocardiographic Characterization of a Murine Model of Hypertrophic Obstructive Cardiomyopathy Induced by Cardiac-specific Overexpression of Epidermal Growth Factor Receptor 2. *Comparative medicine* **66**, 268-277 (2016).

3 Wende, A. R. Post-translational modifications of the cardiac proteome in diabetes and heart failure. *Proteomics. Clinical applications* **10**, 25-38, doi:10.1002/prca.201500052 (2016).

4 Marrocco, V. *et al.* PKC and PKN in heart disease. *Journal of molecular and cellular cardiology* **128**, 212-226, doi:10.1016/j.yjmcc.2019.01.029 (2019).

5 Hanft, L. M. *et al.* Molecule specific effects of PKA-mediated phosphorylation on rat isolated heart and cardiac myofibrillar function. *Archives of biochemistry and biophysics* **601**, 22-31, doi:10.1016/j.abb.2016.01.019 (2016).

6 Bilchick, K. C. *et al.* Heart failure-associated alterations in troponin I phosphorylation impair ventricular relaxation-afterload and force-frequency responses and systolic function. *American Journal of Physiology-Heart and Circulatory Physiology* **292**, H318-H325, doi:10.1152/ajpheart.00283.2006 (2007).

7 Ramirez-Correa, G. A., Cortassa, S., Stanley, B., Gao, W. D. & Murphy, A. M. Calcium sensitivity, force frequency relationship and cardiac troponin I: Critical role of PKA and PKC phosphorylation sites. *Journal of Molecular and Cellular Cardiology* **48**, 943-953, doi:https://doi.org/10.1016/j.yjmcc.2010.01.004 (2010).

8 Meng, F. *et al.* Relationship between cardiac protein tyrosine phosphorylation and myofibrillogenesis during axolotl heart development. *Tissue and Cell* **35**, 133-142, doi:https://doi.org/10.1016/S0040-8166(03)00012-0 (2003).

9 Wade, F., Belhaj, K. & Poizat, C. Protein tyrosine phosphatases in cardiac physiology and pathophysiology. *Heart failure reviews* **23**, 261-272, doi:10.1007/s10741-018-9676-1 (2018).

10 Tartaglia, M. *et al.* Mutations in PTPN11, encoding the protein tyrosine phosphatase SHP-2, cause Noonan syndrome. *Nature Genetics* **29**, 465-468, doi:10.1038/ng772 (2001).

11 Princen, F. *et al.* Deletion of Shp2 tyrosine phosphatase in muscle leads to dilated cardiomyopathy, insulin resistance, and premature death. *Mol Cell Biol* **29**, 378-388, doi:10.1128/mcb.01661-08 (2009).

12 Nguyen, T. D. *et al.* Increased Protein Tyrosine Phosphatase 1B (PTP1B) Activity and Cardiac Insulin Resistance Precede Mitochondrial and Contractile Dysfunction in Pressure-Overloaded Hearts. *Journal of the American Heart Association* **7**, e008865, doi:10.1161/JAHA.118.008865 (2018).

13 Wade, F. *et al.* Deletion of low molecular weight protein tyrosine phosphatase (Acp1) protects against stress-induced cardiomyopathy. *J Pathol* **237**, 482-494, doi:10.1002/path.4594 (2015).

14 Zhang, P. *et al.* Multiple reaction monitoring to identify site-specific troponin I phosphorylated residues in the failing human heart. *Circulation* **126**, 1828-1837, doi:10.1161/CIRCULATIONAHA.112.096388 (2012).

15 Sysa-Shah, P. *et al.* Bidirectional cross-regulation between ErbB2 and β-adrenergic signalling pathways. *Cardiovascular research* **109**, 358-373, doi:10.1093/cvr/cvv274 (2016).
16 Sysa-Shah, P. *et al.* Cardiac-specific over-expression of epidermal growth factor receptor 2 (ErbB2) induces pro-survival pathways and hypertrophic cardiomyopathy in mice. *PloS one* **7**, e42805-e42805, doi:10.1371/journal.pone.0042805 (2012).
17 Vikstrom, K. L., Factor, S. M. & Leinwand, L. A. Mice expressing mutant myosin heavy chains are a model for familial hypertrophic cardiomyopathy. *Molecular medicine (Cambridge, Mass.)* **2**, 556-567 (1996).
18 Lundby, A. *et al.* Quantitative maps of protein phosphorylation sites across 14 different rat organs and tissues. *Nature Communications* **3**, 876, doi:10.1038/ncomms1871 (2012).
19 Sathe, G. *et al.* Phosphotyrosine profiling of human cerebrospinal fluid. *Clinical proteomics* **15**, 29-29, doi:10.1186/s12014-018-9205-1 (2018).
20 Dey, S., DeMazumder, D., Sidor, A., Foster, D. B. & O'Rourke, B. Mitochondrial ROS Drive Sudden Cardiac Death and Chronic Proteome Remodeling in Heart Failure. *Circ Res* **123**, 356-371, doi:10.1161/CIRCRESAHA.118.312708 (2018).
21 Foster, D. B. *et al.* Integrated Omic Analysis of a Guinea Pig Model of Heart Failure and Sudden Cardiac Death. *Journal of Proteome Research* **15**, 3009-3028, doi:10.1021/acs.jproteome.6b00149 (2016).
22 Ayati, M., Erten, S., Chance, M. R. & Koyutürk, M. MOBAS: identification of disease-associated protein subnetworks using modularity-based scoring. *EURASIP journal on bioinformatics & systems biology* **2015**, 7-7, doi:10.1186/s13637-015-0025-6 (2015).
23 Cirillo, E., Parnell, L. D. & Evelo, C. T. A Review of Pathway-Based Analysis Tools That Visualize Genetic Variants. *Front Genet* **8**, 174-174, doi:10.3389/fgene.2017.00174 (2017).
24 Liberzon, A. *et al.* Molecular signatures database (MSigDB) 3.0. *Bioinformatics (Oxford, England)* **27**, 1739-1740, doi:10.1093/bioinformatics/btr260 (2011).
25 Krug, K. *et al.* A Curated Resource for Phosphosite-specific Signature Analysis. *Molecular & cellular proteomics : MCP* **18**, 576-593, doi:10.1074/mcp.TIR118.000943 (2019).
26 Gerull, B. *et al.* Mutations in the desmosomal protein plakophilin-2 are common in arrhythmogenic right ventricular cardiomyopathy. *Nature Genetics* **36**, 1162, doi:10.1038/ng1461(2004).
27 Kapplinger, J. D. *et al.* Distinguishing arrhythmogenic right ventricular cardiomyopathy/dysplasia-associated mutations from background genetic noise. *Journal of the American College of Cardiology* **57**, 2317-2327, doi:10.1016/j.jacc.2010.12.036 (2011).
28 den Haan, A. D. *et al.* Comprehensive desmosome mutation analysis in north americans with arrhythmogenic right ventricular dysplasia/cardiomyopathy. *Circulation. Cardiovascular genetics* **2**, 428-435, doi:10.1161/CIRCGENETICS.109.858217 (2009).
29 Murphy, A. M. & Solaro, R. J. Developmental Difference in the Stimulation of Cardiac Myofibrillar Mg2+-ATPase Activity by Calmidazolium. *Pediatric Research* **28**, 46-47, doi:10.1203/00006450-199007000-00011 (1990).
30 Casado, P. *et al.* Kinase-substrate enrichment analysis provides insights into the heterogeneity of signaling pathway activation in leukemia cells. *Sci Signal* **6**, rs6, doi:10.1126/scisignal.2003573 (2013).

31 Hornbeck, P. V. *et al.* PhosphoSitePlus, 2014: mutations, PTMs and recalibrations. *Nucleic acids research* **43**, D512-D520, doi:10.1093/nar/gku1267 (2015).
32 Wiredja, D. D. *et al.* Phosphoproteomics Profiling of Nonsmall Cell Lung Cancer Cells Treated with a Novel Phosphatase Activator. *Proteomics* **17**, doi:10.1002/pmic.201700214 (2017).
33 Kartasalo, K. *et al.* CytoSpectre: a tool for spectral analysis of oriented structures on cellular and subcellular levels. *BMC Bioinformatics* **16**, 344, doi:10.1186/s12859-015-0782-y (2015).
34 Green, E. M. *et al.* A small-molecule inhibitor of sarcomere contractility suppresses hypertrophic cardiomyopathy in mice. *Science (New York, N.Y.)* **351**, 617-621, doi:10.1126/science.aad3456 (2016).
35 Valachis, A., Nearchou, A., Polyzos, N. P. & Lind, P. Cardiac toxicity in breast cancer patients treated with dual HER2 blockade. *International Journal of Cancer* **133**, 2245-2252, doi:10.1002/ijc.28234 (2013).
36 Peng, K. *et al.* Novel EGFR inhibitors attenuate cardiac hypertrophy induced by angiotensin II. *Journal of cellular and molecular medicine* **20**, 482-494, doi:10.1111/jcmm.12763 (2016).
37 Knöll, R. *et al.* The Cardiac Mechanical Stretch Sensor Machinery Involves a Z Disc Complex that Is Defective in a Subset of Human Dilated Cardiomyopathy. *Cell* **111**, 943-955, doi:https://doi.org/10.1016/S0092-8674(02)01226-6 (2002).
38 Grossmann, K. S. *et al.* Requirement of plakophilin 2 for heart morphogenesis and cardiac junction formation. *The Journal of cell biology* **167**, 149-160, doi:10.1083/jcb.200402096 (2004).
39 Bass-Zubek, A. E. *et al.* Plakophilin 2: a critical scaffold for PKC alpha that regulates intercellular junction assembly. *The Journal of cell biology* **181**, 605-613, doi:10.1083/jcb.200712133 (2008).
40 Tham, Y. K., Bernardo, B. C., Ooi, J. Y., Weeks, K. L. & McMullen, J. R. Pathophysiology of cardiac hypertrophy and heart failure: signaling pathways and novel therapeutic targets. *Archives of toxicology* **89**, 1401-1438, doi:10.1007/s00204-015-1477-x (2015).
41 Hatzivassiliou, G. *et al.* RAF inhibitors prime wild-type RAF to activate the MAPK pathway and enhance growth. *Nature* **464**, 431-435, doi:10.1038/nature08833 (2010).
42 Lorenz, K., Schmitt, J. P., Schmitteckert, E. M. & Lohse, M. J. A new type of ERK1/2 autophosphorylation causes cardiac hypertrophy. *Nat Med* **15**, 75-83, doi:10.1038/nm.1893 (2009).
43 Wang, S. *et al.* Src is required for mechanical stretch-induced cardiomyocyte hypertrophy through angiotensin II type 1 receptor-dependent β-arrestin2 pathways. *PloS one* **9**, e92926-e92926, doi:10.1371/journal.pone.0092926 (2014).
44 Shradhanjali, A., Riehl, B. D., Kwon, I. K. & Lim, J. Y. Cardiomyocyte stretching for regenerative medicine and hypertrophy study. *Tissue Engineering and Regenerative Medicine* **12**, 398-409, doi:10.1007/s13770-015-0010-x (2015).
45 Sachdev, S., Bu, Y. & Gelman, I. H. Paxillin-Y118 phosphorylation contributes to the control of Src-induced anchorage-independent growth by FAK and adhesion. *BMC Cancer* **9**, 12, doi:10.1186/1471-2407-9-12 (2009).
46 Chen, H. *et al.* Temporal and morphological impact of pressure overload in transgenic FHC mice. *Frontiers in Physiology* **4**, doi:10.3389/fphys.2013.00205 (2013).

47 Vakrou, S. *et al.* Allele-specific differences in transcriptome, miRNome, and mitochondrial function in two hypertrophic cardiomyopathy mouse models. *JCI Insight* **3**, doi:10.1172/jci.insight.94493 (2018).
48 Lu, H. *et al.* Integrin-Linked Kinase Expression Is Elevated in Human Cardiac Hypertrophy and Induces Hypertrophy in Transgenic Mice. *Circulation* **114**, 2271-2279, doi:10.1161/CIRCULATIONAHA.106.642330 (2006).
49 Martinez-Ferrando, I. *et al.* Identification of targets of c-Src tyrosine kinase by chemical complementation and phosphoproteomics. *Molecular & Cellular Proteomics*, mcp.M111.015750, doi:10.1074/mcp.M111.015750 (2012).
50 Herbrich, S. M. *et al.* Statistical inference from multiple iTRAQ experiments without using common reference standards. *Journal of proteome research* **12**, 594-604, doi:10.1021/pr300624g (2013).
51 Cox, J. & Mann, M. 1D and 2D annotation enrichment: a statistical method integrating quantitative proteomics with complementary high-throughput data. *BMC Bioinformatics* **13 Suppl 16**, S12, doi:10.1186/1471-2105-13-S16-S12 (2012).
52 Chatr-Aryamontri, A. *et al.* The BioGRID interaction database: 2017 update. *Nucleic Acids Res* **45**, D369-d379, doi:10.1093/nar/gkw1102 (2017).
53 Agrimi, J. *et al.* Obese mice exposed to psychosocial stress display cardiac and hippocampal dysfunction associated with local brain-derived neurotrophic factor depletion. *EBioMedicine* **47**, 384-401, doi:10.1016/j.ebiom.2019.08.042 (2019).

ACKNOWLEDGEMENTS

The project described was supported by Grant Number 5 T32 HL 7227-43 from NIH, R01 HL63038 to AMM, K01-HL13368-01 to GARC, R01 HL13691 to NP and R01 HL088649 to KG. Its contents are solely the responsibility of the authors and do not necessarily represent the official views of the NIH. We thank Dr. Leslie Leinwand for facilitating the Transgenic Mice R403Q-αMyHCTg). This study was partially supported by National Science Foundation of China (81870364) and Shenzhen Sanming Project (SZSM20162057) and Shenzhen Scientific Plan (JCYJ20190809164004023) to MX.

AUTHOR'S CONTRIBUTIONS

MX, XY, XF, AH, XZ, CHN performed experiments, and data analysis, AE, KG, DBF, NP provided statistical support and critical review, KCB, MA provided bioinformatics and statistics support, MX, KCB, NP, AMM and GARC wrote the manuscript, AMM and GARC design the study and supervised the work.

FIGURES AND FIGURE LEGENDS

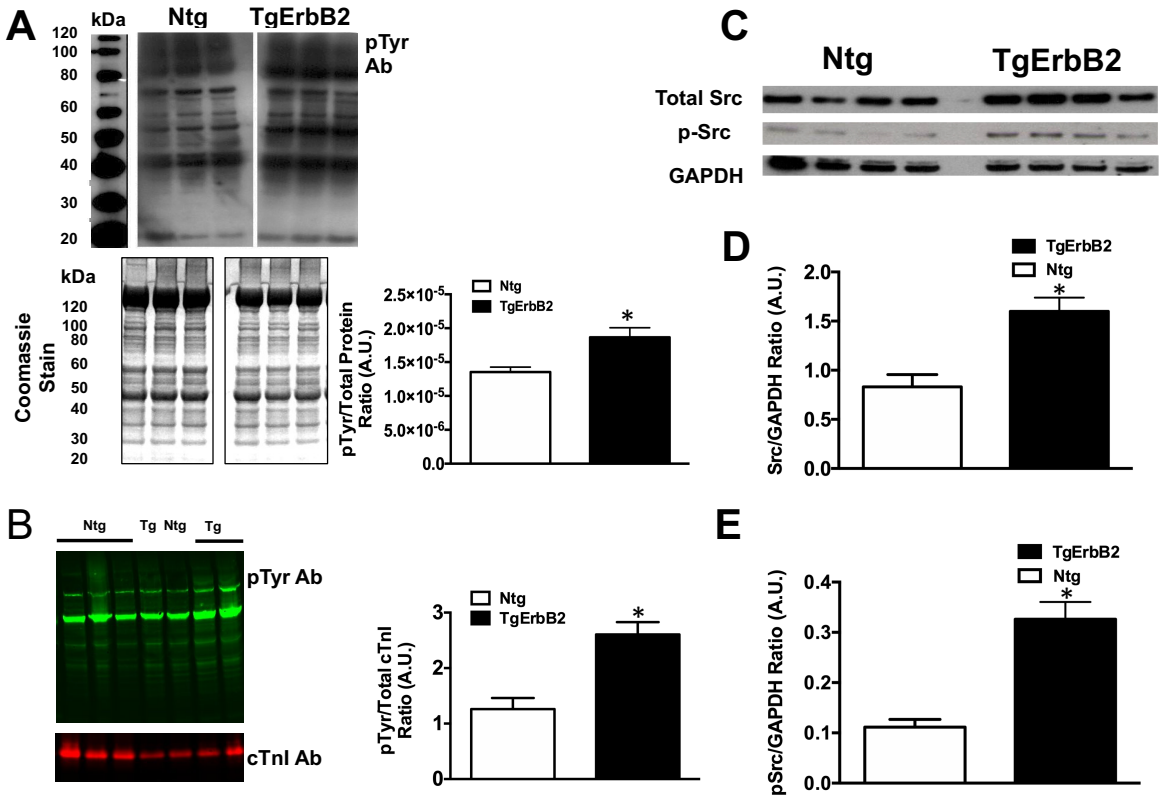

Figure 1

Figure 1. Global Tyrosine phosphorylation and c-Src activation is Enhanced in Cardiac Hypertrophy associated with ErbB2 overexpression. A) Western Blots show increased Tyrosine phosphorylation on TgErbB2 mice heart homogenates (Top Panel). Corresponding total protein loading by Coomassie Blue Staining is shown on the lower panel. **B)** Fluorescence densitometry analysis shows that after pTyrosine signal (IRDye® 800CW) was normalized to total cTnI (IRDye® 680 LT), the TgErbB2 mice had a significant increase (2.61±0.22 vs. 1.26±0.2, $p<0.05$). **C)** Western Blots show expression levels of total Src and p-Src (Tyr 416) and GAPDH as loading control. **D), E)** Densitometry analysis revealed that Src levels are elevated in TgErbB2, and p-Src phosphorylation levels are elevated. Signals were normalized to total GAPDH. However, this finding is also influenced by the significant increase in total Src expression on TgErbB2 mice.

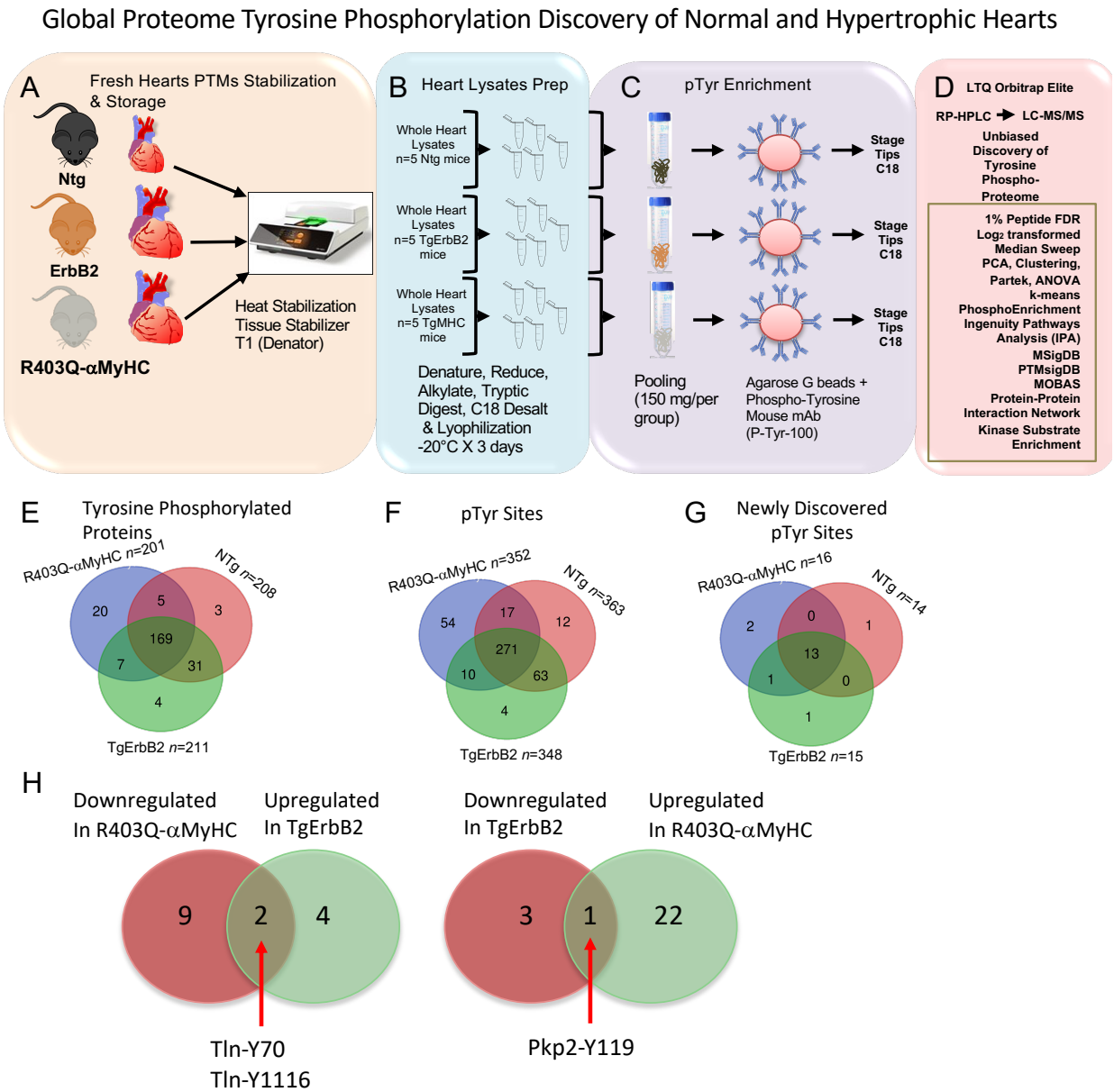

Figure 2

Figure 2. Workflow for Global Tyrosine Phosphorylation Profiling by Label-Free Proteomics. A) Ventricular tissues were rinsed with PBS and subjected to Heat Stabilization using a T1 Tissue Stabilizor (Denator, Sweden) to maximize phosphorylation preservation, then snap -frozen in liquid nitrogen and stored at -80°C until further use. **B)**

Ntg, TgErbB2, and R403Q-αMyHC mice hearts (*n*=5 per group) were processed in parallel to obtain whole heart lysates; 30 mg of protein lysates were used from each mouse heart for an in-solution trypsin digestion, a total of 150 mg of trypsinized protein per genotype were C18 desalted and lyophilized at –20°C for three days. **C)** A total of 150 mg of tryptic peptides (pooled material from 5 hearts per group) were enriched for pTyrosine using immunoaffinity precipitation (Protein Agarose Beads + 300 micrograms of mAb Anti-pTyr) and desalted on C18 stage tips. **D)** RP-HPLC ESI (electrospray ionization) MS/MS was performed on an LTQ Orbitrap Elite (Thermo Scientific) for a 120 min on a linear acetonitrile gradient (4−40%). Raw data were searched with Mascot 2.3, and label-free quantification with MS1 extracted ion chromatograms were performed using MaxQuant. This approach was repeated three times with samples from all three groups run in parallel; 15 hearts per genotype in three technical replicates.

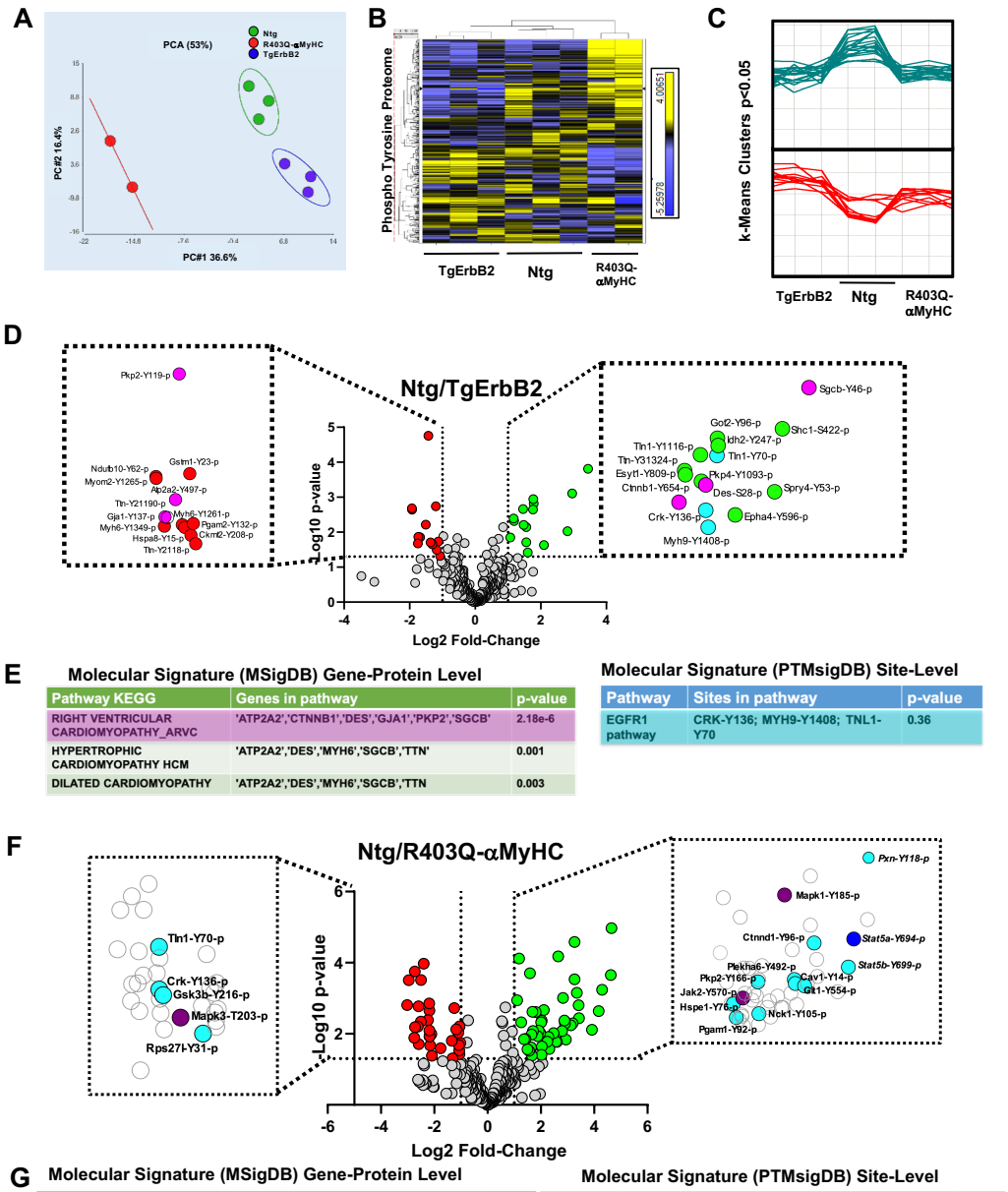

Pathway KEGG	Genes in pathway	p-value
RIGHT VENTRICULAR CARDIOMYOPATHY_ARVC	'ATP2A2','CTNNB1','DES','GJA1','PKP2','SGCB'	2.18e-6
HYPERTROPHIC CARDIOMYOPATHY HCM	'ATP2A2','DES','MYH6','SGCB','TTN'	0.001
DILATED CARDIOMYOPATHY	'ATP2A2','DES','MYH6','SGCB','TTN	0.003

Pathway	Sites in pathway	p-value
EGFR1 pathway	CRK-Y136; MYH9-Y1408; TNL1-Y70	0.36

Pathway KEGG	Genes in pathway	p-value
Focal ADHESION	'CAV1','CRK','FLT1','GSK3B','KDR','MAPK1','MAPK3','PTK2','PXN','TLN1'	0.02
PID VEGFR1-2 PATHWAY	'CAV1','FLT1','HSP90AB1','KDR','MAPK1' ,'MAPK3', 'NCK1','PTK2','PXN'	0.01
ERBB Signaling Pathway	'CRK','GSK3B','MAPK1','MAPK3','NCK1','PTK2','STAT5A', 'STAT5B'	0.002
CHEMOKINE Signaling Pathway	'CRK','GSK3B','JAK2','MAPK1','MAPK3','PTK2','PXN','STAT5B'	0.005
PID ANGIOPOETIN RCEPTOR PATHWAY	'CRK','MAPK1','MAPK3','NCK1','PTK2','PXN','STAT5A','STAT5B'	0.005

Pathway	Sites in pathway	p-value
EGFR1 pathway	'CAV1-Y14','CRK-Y136','CTNND1-Y96','GIT1-Y554','GSK3B-Y216','HSPE1-Y76','NCK1-Y105','PGAM1-Y92','PKP2-Y166,,'PLEKHA6-Y492','PTK2-Y576','PXN-Y118','RPS27L-Y31,'STAT5A-Y694','STAT5B-Y699','TLN1-Y70'	0.001
PERT_PSP_EPO	'JAK2-Y570','MAPK1-Y185','MAPK3-T203','STAT5A-Y694'	5.6E-4

Figure 3

Figure 3. PTMSigDB Reveals Distinct Tyrosine Phosphorylation Signatures of Cardiac Proteome in Hypertrophic Cardiomyopathy Models. A) Unsupervised principal component analysis (PCA) of Non-transgenic, TgErbB2, and R403Q-αMyHC mice shows distinct experimental groups' distinct segregation. The full cardiac proteome was enriched for pTyrosine peptides; their logged and summarized signal intensities

indicate that the groups segregate along with the first principal component (PC #1), which accounts for 36.6% of the total correlation in the expression of Phospho Tyrosine Proteome (normalized, mean=0, variance=1). The group of R403Q-αMyHC (red) is the most distinct of the three proteomes, whereas the TgErbB2 (blue) and Normal (green) heart proteomes differ more marginally. **B)** A heatmap was used to visualize the unsupervised hierarchical clustering of proteins with p-value <0.05 by ANOVA. Overrepresented (yellow) and underrepresented (Blue). **C**) K-means clustering was used to parse the phospho-tyrosine proteome by signal intensity into groups whose expression changed in TgErbB2 and R403Q-αMyHC relative to the Ntg group. Four clusters were made with the proteins that displayed p-value and q-value < 0.05 using correlation as similarity measurement, for representation only Cluster 1 (Score:10.47) on the top and Cluster 3 (Score: 16.37) on the bottom are shown. **D)** Volcano plot showing the Log2 fold-change and –Log10 p-value of each pTyr peptide in the pairwise comparison of Ntg and TgErbB2. The dots highlighted in red depict the sites which showed a significantly lower intensity, whereas the dots in green highlight the sites with significantly higher intensity (p-value <0.05, FC >2). A magnification of the significant sites was made at the figure (dotted squares) to label the peptide site. **E)** Molecular Signature DB (MSigDB) and Molecular PTMs Signature DB (PTMsigDB) of Global pTyrosine Phosphorylation data identified pathways that were significantly altered. **F)** Volcano plot showing the Log2 fold-change and –Log10 p-value of each pTyr peptide in the pairwise comparison of Ntg and R403Q-αMyHC. The dots highlighted in red depict the sites which showed a significantly lower intensity, whereas the dots in green highlight the sites with significantly higher intensity (p-value <0.05, FC >2). A magnification of the significant sites was made at the figure (dotted squares) to label in cyan color for members of EGFR1 Pathway and in purple color for EPO stimulation (PSP_EPO) memberrs by PTMsigDB.

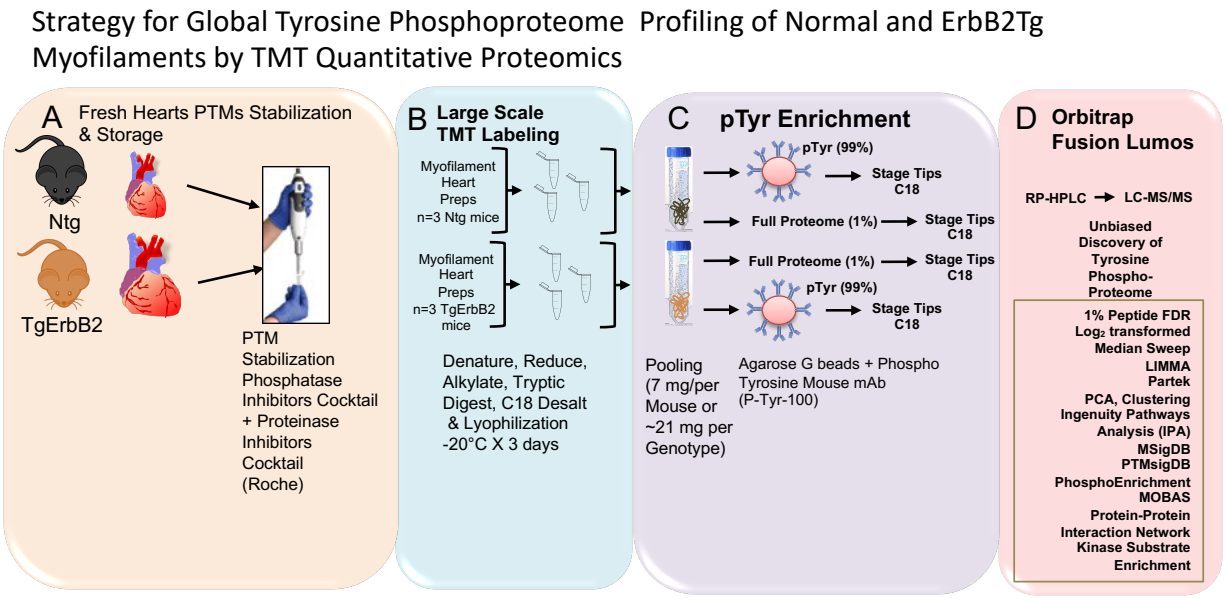

Figure 4

Figure 4. Workflow for Global Tyrosine Phosphorylation Identification of Normal and TgErbB2 Hypertrophic Myofilaments by TMT Quantitative Proteomics. A) Myofilament from Ntg (*n*=3) and ErbB2 (*n*=3) transgenic mice hearts were freshly isolated on ice-cold buffers containing Proteinase and Phosphatase Inhibitors Cocktails (Roche). **B)** All material was resuspended in TEAB, followed by reduction and alkylation. Tryptic peptides were desalted and labeled with 6-plex isobaric tandem mass tags (TMT). **C)** The digested and labeled peptides were pooled and desalted with C_{18} SEP-PAK. The enrichment for phosphotyrosine was performed with PTMScan Phospho-Tyrosine Rabbit mAb (P-Tyr-1000) kit (Cell Signaling Technology). The eluted peptide samples were desalted using C18 STAGE tips **D)** Easy-nanoLC 1200 nanoflow liquid chromatography system coupled to Orbitrap Fusion Lumos Tribrid.

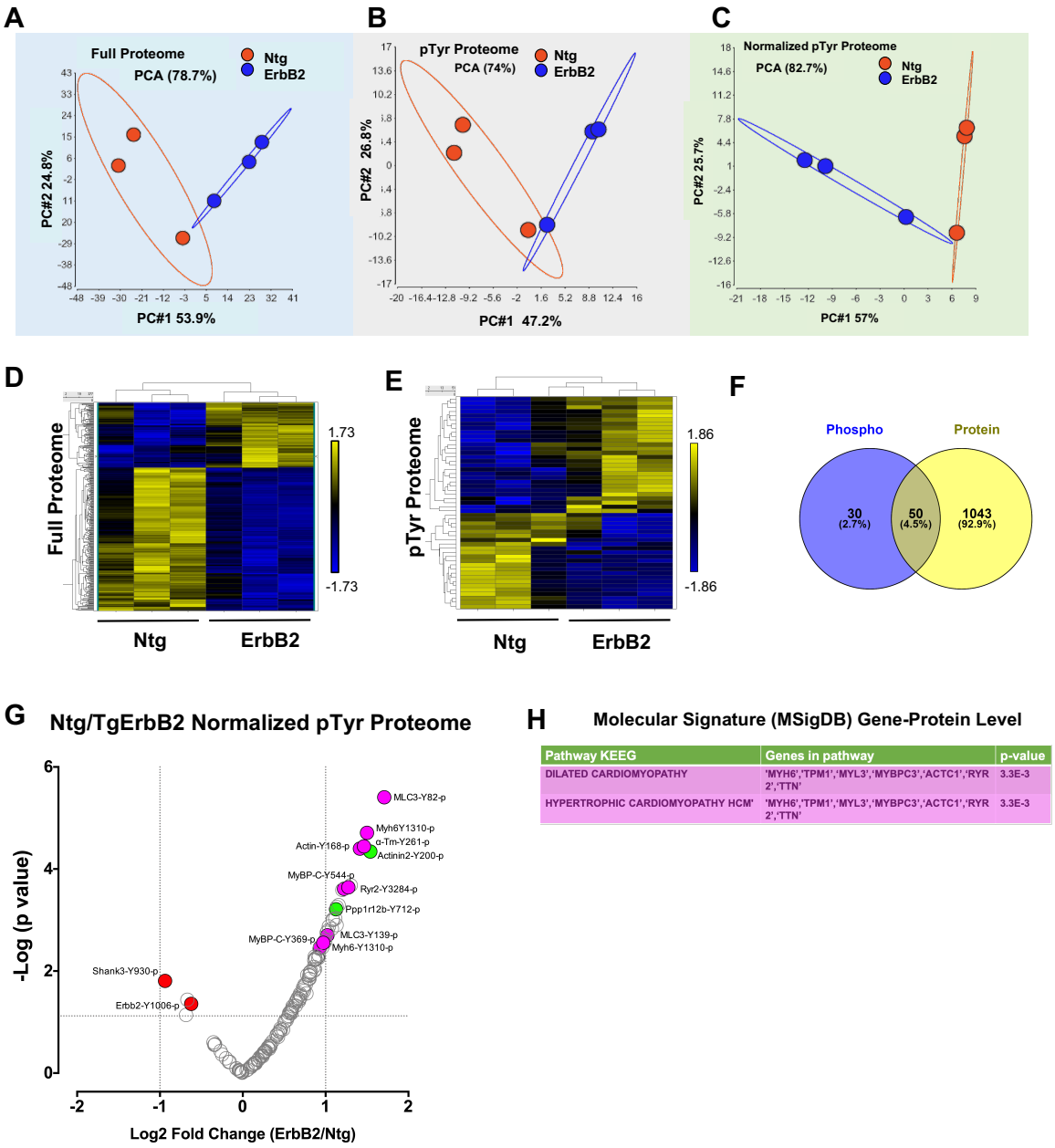

Pathway KEEG	Genes in pathway	p-value
DILATED CARDIOMYOPATHY	'MYH6','TPM1','MYL3','MYBPC3','ACTC1','RYR2','TTN'	3.3E-3
HYPERTROPHIC CARDIOMYOPATHY HCM'	'MYH6','TPM1','MYL3','MYBPC3','ACTC1','RYR2','TTN'	3.3E-3

Figure 5

Figure 5. TgErbB2 Cardiac Sarcomere pTyrosine Proteome Remodeling. A) Full Proteome was labeled with TMT, and the logged and summarized protein signal intensities indicate that experimental groups segregate along with the first principal component (PC #1), which accounts for 53.9% of the total correlation in the expression proteome (normalized, mean=0, variance=1). **B)** PCA of the phospho-Tyr proteome reveals a similar trend, and the groups segregate along the PC#1, which accounts for

47.2% of the correlation. **C)** Signal intensities of the phospho-Tyr proteome were normalized to Full Proteome protein expression and analyzed by principal component analysis. The distinctive signature of pTyr is still apparent by PC along PC#1 and accounts for 57% of the correlation. **D)** A heatmap was used to visualize the unsupervised hierarchical correlation clustering of protein expression and **E)** pTyr Proteome expression with $p<0.05$ by LIMMA moderated 2-samples t-test comparison of TgErbB2 and Ntg group. **F)** pTyr Phosphopeptides were matched to Proteins identified in the Full Proteome set of peptides; the overlap did not vary significantly between matching pTyr Phospho peptides to a Protein accession number or a Gene ID (Venn Diagram is shown). **G)** Volcano plot showing the Log2 fold-change and –Log10 p-value of each pTyr peptide in the pairwise comparison of Ntg and TgErbB2. The dots highlighted in red depict the sites which showed a significantly lower intensity, whereas the dots in green highlight the sites with significantly higher intensity (fold-change >0.5, p-value <0.05, and q-value <0.05). For clarity of presentation, only some peptides were highlighted. **H)** Molecular Signature DataBase (MSigDB) confirmed targets and the involvement of Dilated and Hypertrophic cardiomyopathy KEEG Pathways also found on the label-free approach for TgErbB2 mice.

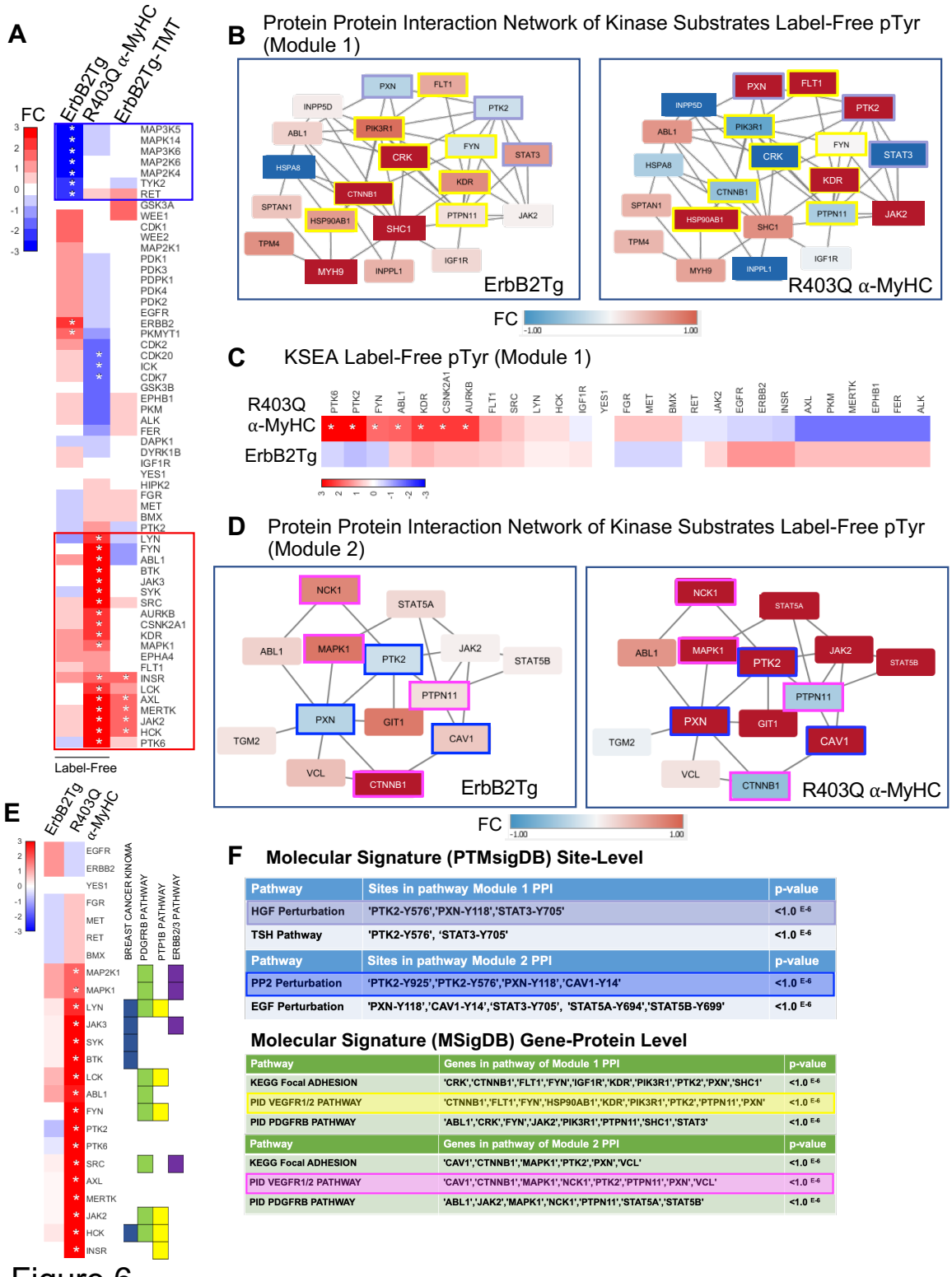

Figure 6

F **Molecular Signature (PTMsigDB) Site-Level**

Pathway	Sites in pathway Module 1 PPI	p-value
HGF Perturbation	'PTK2-Y576','PXN-Y118','STAT3-Y705'	<1.0 E-6
TSH Pathway	'PTK2-Y576', 'STAT3-Y705'	<1.0 E-6
Pathway	**Sites in pathway Module 2 PPI**	**p-value**
PP2 Perturbation	'PTK2-Y925','PTK2-Y576','PXN-Y118','CAV1-Y14'	<1.0 E-6
EGF Perturbation	'PXN-Y118','CAV1-Y14','STAT3-Y705', 'STAT5A-Y694','STAT5B-Y699'	<1.0 E-6

Molecular Signature (MSigDB) Gene-Protein Level

Pathway	Genes in pathway of Module 1 PPI	p-value
KEGG Focal ADHESION	'CRK','CTNNB1','FLT1','FYN','IGF1R','KDR','PIK3R1','PTK2','PXN','SHC1'	<1.0 E-6
PID VEGFR1/2 PATHWAY	'CTNNB1','FLT1','FYN','HSP90AB1','KDR','PIK3R1','PTK2','PTPN11','PXN'	<1.0 E-6
PID PDGFRB PATHWAY	'ABL1','CRK','FYN','JAK2','PIK3R1','PTPN11','SHC1','STAT3'	<1.0 E-6
Pathway	**Genes in pathway of Module 2 PPI**	**p-value**
KEGG Focal ADHESION	'CAV1','CTNNB1','MAPK1','PTK2','PXN','VCL'	<1.0 E-6
PID VEGFR1/2 PATHWAY	'CAV1','CTNNB1','MAPK1','NCK1','PTK2','PTPN11','PXN','VCL'	<1.0 E-6
PID PDGFRB PATHWAY	'ABL1','JAK2','MAPK1','NCK1','PTPN11','STAT5A','STAT5B'	<1.0 E-6

Figure 6. Kinase Substrate Enrichment Analysis & MoBaS Analysis. A) KSEA on label-free pTyr enrichment and TMT pTyr Enrichment data. Heat maps report KSEA

results according to normalized scores (i.e., TgErbB2/Ntg, R403Q-αMyHC/Ntg, etc.). Only kinases shared between data sets are included, therefore present in Tg and Ntg. Asterisks indicate the statistical significance of $p < 0.05$. Red represents a positive score and blue a negative score. Red rectangle highlights groups of activated kinases that clustered together and are predominant in R403Q-αMyHC, whereas the blue rectangle highlights suppressed kinases that clustered and are predominant on TgErbB2. **B)** MoBaS identified a tightly interconnected subnetwork involved in growth factors signaling (VEGF1/2 and Hepatocyte Growth Factor). Represented by the top-scoring Protein-Protein Interaction (PPI) subnetwork called Module 1 was identified on TgErbB2 label-free and compared to R403Q-αMyHC. **C)** KSEA on Module 1 group of substrates. **D)** Second top-scoring PPI subnetwork called Module 2 identified on R403Q-αMyHC label-free and compared to TgErbB2. **E)** KSEA on Module 2 group of substrates and associated pathways and specific kinases are denoted with colored squares. **F)** Results from PTMsigDB and MSigDB analysis. Color code highlight the pathway and the substrate involved in the Modules 1 or 2. On PPI modules, each node is a phosphoprotein represented by its most significant peptide. Node color is based on Log2 fold-change relative to NTG. The scale is noted by FC and a bar colored from blue to red.

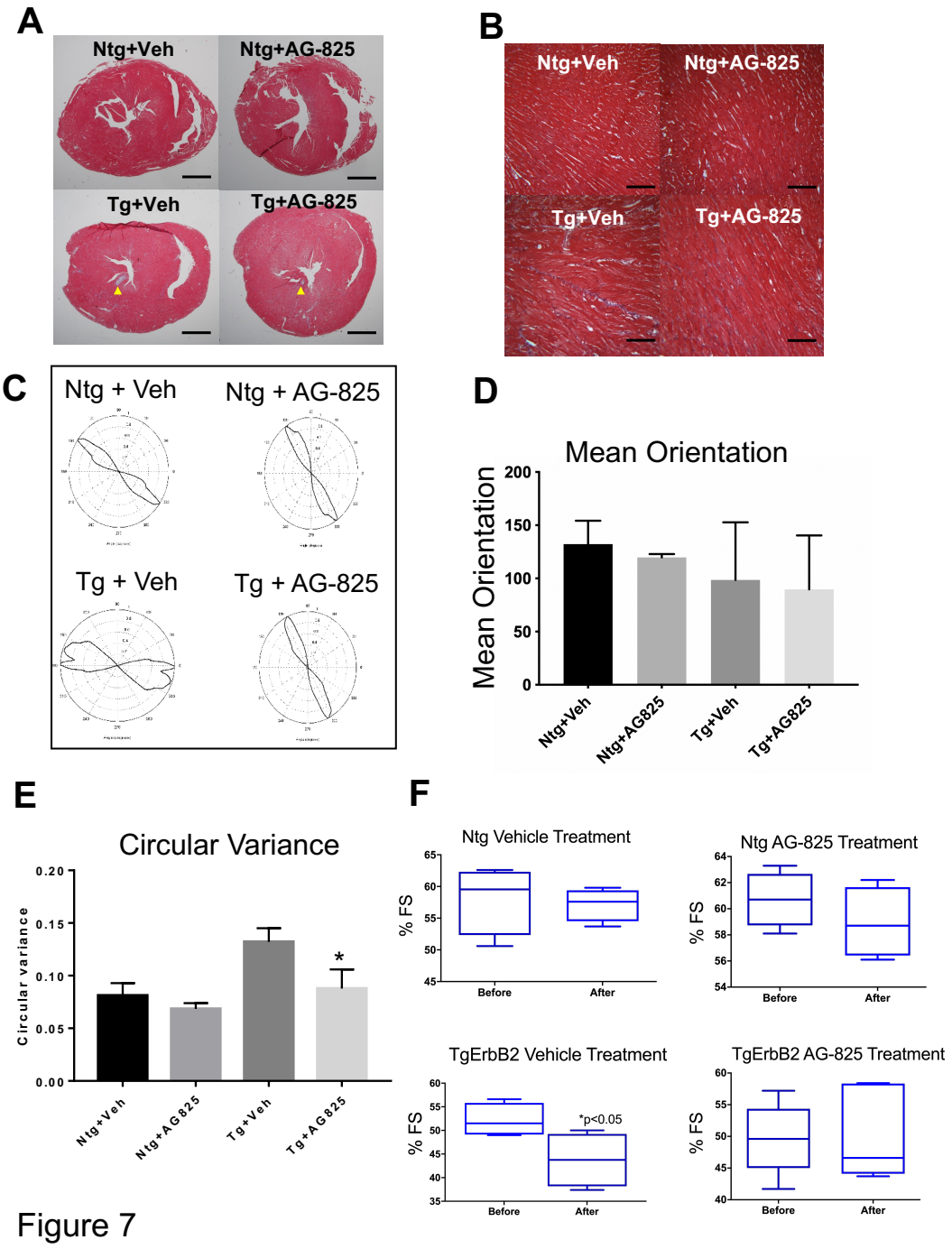

Figure 7

Figure 7. Tyrosine Kinase receptor Inhibitor AG-825 reduces Cardiac Myocyte Disarray and Preserves Contractile Function in TgErbB2 Mice. A) Masson's trichrome stained sections (5X) from vehicle-treated Ntg and AG-825–treated Ntg (top panel) and vehicle-treated TgErbB2 and AG-825-treated TgErbB2 mice (lower panel),

yellow arrowheads point to fibrotic areas. Scale bar 1 mm. **B)** Masson's trichrome stained sections (40X) from representative regions of interest (ROI) show increased Fibrosis in TgErbB2 mice myocardium (Bottom left panel), that fibrosis improved after 2-weeks of AG-825 Treatment. The same areas were used to determine the level of cardiac myocyte disarray. This was achieved by analyzing cell orientation using CytoSpectre Software from Vehicle and AG-825 treated Ntg and TgErbB2 mouse heart sections (scale bar 50μm). **C)** Plots of the distribution of cardiac cells orientation angles. Note how Ntg angles are homogeneous and did not change in the group treated with AG-825 (Top panel). In contrast, Tg treated with vehicle showed less homogenous and different orientation angle, which confirms cardiomyocyte disarray (bottom left panel). AG-825 treatment reduces cardiomyocyte disarray, and the orientation plot is similar to AG-825 treated NTG group. **D)** Mean orientation angle of cardiac myocytes, and **E)** Circular variance, another measure of isotropy, in Ntg and TgErbB2 mice with and without AG-825 treatment (*n*= 5 animals per condition). Graph bars are expressed as mean ± SD; the ANOVA test performed statistical comparisons showing a significant improvement of TgErbB2 mice treated with AG-825 (p-value<0.05). **F)** Cardiac echocardiography from the four groups demonstrates that AG-825 treatment for 14 days preserved the contractile function, estimated as % Fraction Shortening and % Ejection Fraction (not shown), in TgErbB2 mice (Lower right panel). In contrast, TgErbB2 mice treated with the vehicle deteriorated significantly (Lower left panel, paired t-test, p-value<0.05). Ntg mice contractility was not affected by vehicle or AG-825 Treatment (Upper Panels).